

Helicoidal Transformation Method for Finite Element Models of Twisted Superconductors

Julien Dular, François Henrotte, André Nicolet, Mariusz Wozniak, Benoît Vanderheyden, and Christophe Geuzaine

Abstract—This paper deals with the modelling of superconducting and resistive wires with a helicoidal symmetry, subjected to an external field and a transport current. Helicoidal structures are three-dimensional, and therefore yield computationally intensive simulations in a Cartesian coordinate system. We show in this paper that by working instead with a helicoidal system of coordinates, the problem to solve can be made two-dimensional, drastically reducing the computational cost. We first introduce the state-of-the-art approach and apply it on the h - ϕ -formulation with helicoidally symmetric boundary conditions (e.g., axial external magnetic field, with or without transport current), with an emphasis on the function space discretization. Then, we extend the approach to general boundary conditions (e.g., transverse external magnetic field) and we present numerical results with linear materials. In particular, we discuss the frequency-dependent losses in composite wires made of superconducting filaments embedded in a resistive matrix. Finally, we provide outlook to the application of the generalized model with nonlinear materials.

I. INTRODUCTION

LOW-TEMPERATURE superconducting composite wires usually consist of a large number of superconducting filaments embedded in a conducting matrix. This matrix helps in redistributing current between filaments, but has the side effect of coupling the filaments in the presence of an external transverse time-varying magnetic field. This coupling can however be reduced by twisting the composite wire [1], [2]. The resulting geometry is not invariant along the wire axis and leads to a computationally intensive three-dimensional (3D) modelling [3], [4], [5], [6].

Approximate models exploiting the multifilamentary structure of this kind of wires have been investigated to reduce the computational cost, such as in [7] and [8], where coupling currents in the conducting matrix are accounted for in a 2D finite element model by introducing equivalent resistances between the filaments. Alternatively, a Frenet frame is used in [9] to simplify the definition of the 3D geometry, and AC losses are approximated by considering a fraction of the pitch length of the wire in a 3D model, or a cross section of the wire in a 2D model. Homogenization techniques involving anisotropic materials have also been considered [3]. Finally, parallelization methods are considered to reduce the computational time [6].

Whenever possible, it is always recommended to exploit existing symmetries. In particular, the dimension of a problem presenting a helicoidal symmetry, i.e., a combination of

translational and rotational symmetries with the same axis, can be reduced from 3D to 2D without loss of accuracy if the calculations are performed in a *helicoidal coordinate system*. Methods based on this coordinate transformation have first been introduced in optical waveguide simulations [10], [11], [12], and since then applied to electrostatic problems [13], [14], linear magnetodynamic problems [15], [16], [17], and nonlinear magnetodynamic problems with superconducting filaments or tapes [18], [19], [20], [21].

An exact helicoidal symmetry is rarely encountered in practical applications, but different kinds of deformed geometries, curved wires, or conductor organized, e.g., into layers with distinct twist pitch lengths, may exhibit an approximate or partial helicoidal symmetry. Working with helicoidal coordinate systems can still be very useful in such cases, especially in the context of a multi-scale or a sub-problem approach, to compute homogenized parameters that account for the twisting of the filaments (e.g., Rutherford multistrand cables). Furthermore, the 2D helicoidal approach is more accurate than an equivalent 3D approach, as the latter is usually limited in accuracy by non-conformities at element interfaces in unstructured 3D meshes. Extensions and improvements of the helicoidal method are therefore currently being investigated, e.g., in [16], to quantify helicoidal effects in the context of Litz wires.

This paper focuses on the helicoidal transformation method. We start the analysis in Section II by applying the change of coordinates to the h - ϕ -formulation [22], which is an efficient formulation for systems with superconductors [23], and we then state the mathematical conditions for reducing the problem dimension from 3D to 2D. We will refer to the equations resulting from this analysis as the 2D- ξ model, in order to emphasize the fact that it is solved in helicoidal coordinates. As will be shown, a feature of the 2D- ξ model, compared to a conventional 2D model in Cartesian coordinates, is that it solves for fields with three independent components, instead of two.

Depending on the symmetry of the boundary conditions (BC), the study is decomposed in two cases. If the magnetic field excitation is axial and uniform, the BC then also verify the helicoidal symmetry, irrespective of whether there is a transport current or not. The dimension of this problem (geometry plus BC), being helicoidally symmetric, can be reduced from 3D to 2D by simply applying the coordinate transformation method. This approach is not new in the context of superconducting wires [18], [19], [20], but it has not yet been presented with the efficient h - ϕ -formulation. In Section III, the implementation details of this formulation are reviewed with an emphasis on the discretization of a curl-free

J. Dular and M. Wozniak are with CERN, Geneva, Switzerland. A. Nicolet is with the Aix-Marseille University, France. F. Henrotte, B. Vanderheyden, and C. Geuzaine are with the University of Liège, Belgium.

magnetic field in non-conducting domains. In Section IV, the implementation is verified by comparison with a 3D model in Cartesian coordinates.

If the magnetic field excitation is transverse, then the BC are no longer helicoidally symmetric. A generalization of the method is proposed in Section V for this case. It still results in a 2D model in some situations. To the best of our knowledge, this generalization is a novelty compared to state-of-the-art methods. Attention is again paid to the curl-free property of the magnetic field in non-conducting domains. The generalized model is applied to linear materials in Section VI, and it is shown that it reproduces the predictions of analytical models for the coupling currents [2]. We finally provide a brief prospect about the application of the generalized method in the presence of nonlinear materials.

All presented models are implemented in and solved by GetDP [24]. Geometry and mesh generation are performed by Gmsh [25]. All codes are open-source and available in the Life-HTS toolkit¹.

II. HELICOIDAL CHANGE OF COORDINATES

Let (x, y, z) be a Cartesian coordinate system. The *helicoidal change of coordinates* $x \rightarrow \xi$ and its inverse $\xi \rightarrow x$ read [11]

$$\begin{cases} \xi_1 = x \cos(\alpha z) + y \sin(\alpha z), \\ \xi_2 = -x \sin(\alpha z) + y \cos(\alpha z), \\ \xi_3 = z, \end{cases} \quad (1)$$

and

$$\begin{cases} x = \xi_1 \cos(\alpha \xi_3) - \xi_2 \sin(\alpha \xi_3), \\ y = \xi_1 \sin(\alpha \xi_3) + \xi_2 \cos(\alpha \xi_3), \\ z = \xi_3, \end{cases} \quad (2)$$

respectively, with (ξ_1, ξ_2, ξ_3) the helicoidal coordinate system. The twisting parameter $\alpha \in \mathbb{R}$ is the unique parameter of the coordinate transformation, and the pitch length is $p = 2\pi/\alpha$.

With this transformation, helices of pitch length p around the z -axis in the Cartesian coordinate system are mapped into straight lines parallel to the ξ_3 -axis in the helicoidal coordinate system. This is illustrated in Fig. 1 with $p = 1$. A geometry is said to be helicoidally symmetric, or to have a helicoidal symmetry, if there exists a value α for which its description in helicoidal coordinates is ξ_3 -invariant, i.e., independent of ξ_3 .

The Jacobian matrix \mathbf{J} of the coordinate transformation Eq. (2) reads

$$\mathbf{J} = \frac{\partial x_i}{\partial \xi_j} = \begin{pmatrix} c & -s & -\alpha \xi_1 s - \alpha \xi_2 c \\ s & c & \alpha \xi_1 c - \alpha \xi_2 s \\ 0 & 0 & 1 \end{pmatrix}, \quad (3)$$

with $s = \sin(\alpha \xi_3)$ and $c = \cos(\alpha \xi_3)$. We have $\det \mathbf{J} = 1$. The inverse transposed Jacobian matrix \mathbf{J}^{-T} , written in terms of the ξ -coordinates, then reads

$$\mathbf{J}^{-T} = \frac{\partial \xi_j}{\partial x_i} = \begin{pmatrix} c & -s & 0 \\ s & c & 0 \\ \alpha \xi_2 & -\alpha \xi_1 & 1 \end{pmatrix}. \quad (4)$$

¹Available: www.life-hts.uliege.be.

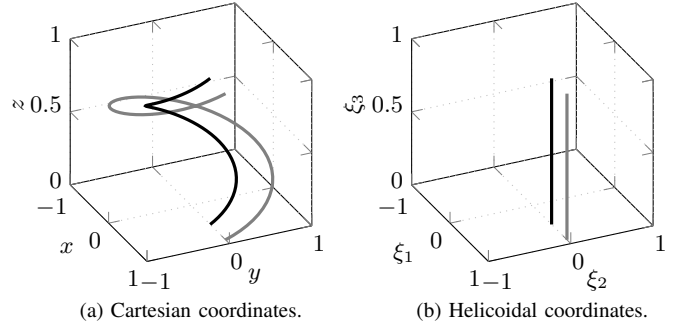


Fig. 1: Transformation of two helicoidal curves with the change of coordinates Eq. (1) with $\alpha = 2\pi$.

A. Helicoidal transformation of fields

The Jacobian matrix describes the mapping of vector components with the transformation. Components of one-forms, such as the magnetic field \mathbf{h} , follow the transformation [10], [26]

$$\mathbf{h}_x = \mathbf{J}^{-T} \mathbf{h}_\xi, \quad (5)$$

where \mathbf{h}_x and \mathbf{h}_ξ denote the components of the field \mathbf{h} in the Cartesian and helicoidal coordinate systems, respectively.

Components of two-forms, such as the current density \mathbf{j} ($= \mathbf{curl} \mathbf{h}$), follow the transformation [10], [26]

$$\mathbf{j}_x = \frac{\mathbf{J}}{\det \mathbf{J}} \mathbf{j}_\xi, \quad (6)$$

where \mathbf{j}_x and \mathbf{j}_ξ denote the components of the field \mathbf{j} in the Cartesian and helicoidal coordinate systems, respectively.

B. Problem definition and h - ϕ -formulation

The eddy current problem is governed by the following magnetodynamic (or magneto-quasistatic) equations and constitutive laws [27]:

$$\begin{cases} \operatorname{div} \mathbf{b} = 0, \\ \operatorname{curl} \mathbf{h} = \mathbf{j}, \\ \operatorname{curl} \mathbf{e} = -\partial_t \mathbf{b}, \end{cases} \quad \text{and} \quad \begin{cases} \mathbf{b} = \mu \mathbf{h}, \\ \mathbf{e} = \rho \mathbf{j}, \end{cases} \quad (7)$$

with \mathbf{b} , \mathbf{h} , \mathbf{j} , \mathbf{e} , μ , and ρ , the magnetic flux density (T), the magnetic field (A/m), the current density (A/m²), the electric field (V/m), the permeability (H/m), and the resistivity (Ωm), respectively. In non-conducting materials, $\rho \rightarrow \infty$ and $\mathbf{j} = \mathbf{0}$, and Ampère's law reads

$$\operatorname{curl} \mathbf{h} = \mathbf{0}. \quad (8)$$

In this paper, special attention is paid to satisfy this condition.

Type-II irreversible superconductors are characterized by a nonlinear electric response. Assuming isotropy for low-temperature superconductors, their resistivity is given by the power law [28],

$$\rho_{\text{SC}} = \frac{e_c}{j_c} \left(\frac{\|\mathbf{j}\|}{j_c} \right)^{n-1}, \quad (9)$$

where $e_c = 10^{-4}$ V/m is an electric field threshold defining the critical current density j_c (A/m²), and n (-) describes the sharpness of the transition to flux flow. The norm of \mathbf{j} is

denoted by $\|\mathbf{j}\|$, with $\|\mathbf{j}\|^2 = j_x^2 + j_y^2 + j_z^2$ in the Cartesian coordinates. Finally, all materials are assumed to be non-magnetic, so that one has $\mu = \mu_0 = 4\pi \times 10^{-7}$ H/m in all domains.

The magnetodynamic problem defined above is solved in a computational domain Ω . Let Ω be a helicoidally symmetric domain. It consists of a conducting domain Ω_c made of N connected subdomains, $\Omega_c = \cup_{i \in C} \Omega_{c_i}$, with $C = \{1, \dots, N\}$, surrounded by a non-conducting domain Ω_c^c . The external boundary of Ω is noted Γ_{out} . Via boundary conditions (BC), the system can be subjected to a given axial magnetic field $\mathbf{h}_{\text{axial}}$ and/or a given transverse magnetic field $\mathbf{h}_{\text{trans}}$. A transport current \bar{I}_i is imposed to the subdomains Ω_{c_i} for $i \in C_I \subset C$, and a voltage \bar{V}_i is imposed on the subdomains Ω_{c_i} for $i \in C \setminus C_I = C_V$. We shall call *global conditions* (GC) these electric conditions imposed to the conductors of the system. Fig. 2 represents a typical cross section of the problem at hand.

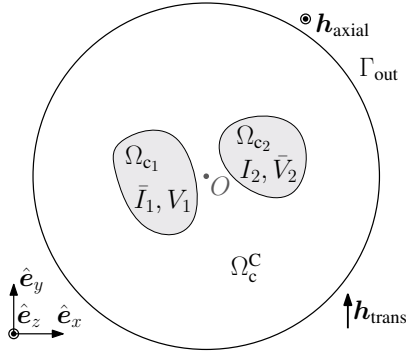


Fig. 2: 2D cross section of the problem. Boundary conditions (BC) are axial magnetic field $\mathbf{h}_{\text{axial}}$ and transverse magnetic field $\mathbf{h}_{\text{trans}}$ imposed on Γ_{out} . Global conditions (GC) are applied transport current \bar{I}_1 on Ω_{c_1} , and applied voltage \bar{V}_2 on Ω_{c_2} . In this example, $C = \{1, 2\}$, $C_I = \{1\}$, and $C_V = \{2\}$. The 3D geometry is the rotated extrusion of the represented 2D cross section.

We solve the problem defined above with the finite element method. Among the existing finite element formulations, we choose the h - ϕ -formulation [22]. It involves the power law written in terms of the resistivity, which has been shown to lead to robust and efficient numerical resolutions for problems involving superconductors characterized by the power law [23]. Also, the h - ϕ -formulation strongly verifies the curl-free condition on \mathbf{h} in Ω_c^c , Eq. (8), by expressing the magnetic field as the gradient of a scalar potential. This leads to a lower number of degrees of freedom compared to the h -formulation [30], that uses instead a spurious non vanishing resistivity to limit the current density in Ω_c^c .

The 3D h - ϕ -formulation reads [23]: from an initial solution at $t = 0$, find $\mathbf{h} \in \mathcal{H}(\Omega)$ such that, for $t > 0$ and $\forall \mathbf{h}' \in \mathcal{H}_0(\Omega)$, we have

$$(\partial_t(\mu \mathbf{h}), \mathbf{h}')_{\Omega} + (\rho \mathbf{curl} \mathbf{h}, \mathbf{curl} \mathbf{h}')_{\Omega_c} = \sum_{i \in C_V} \bar{V}_i \mathcal{I}_i(\mathbf{h}'). \quad (10)$$

The integral over Ω of the inner product of \mathbf{f} and \mathbf{g} is denoted by $(\mathbf{f}, \mathbf{g})_{\Omega}$, whereas the operator $\mathcal{I}_i(\mathbf{h})$ gives the circulation of \mathbf{h} around conductor i , which is the net current I_i flowing

in the conductor. The associated voltage is noted \bar{V}_i . The function space $\mathcal{H}(\Omega)$ is the subspace of $H(\mathbf{curl}; \Omega)$ containing functions that are curl-free in Ω_c^c and verify the essential BC and the GC [21]. The space $\mathcal{H}_0(\Omega)$ is the same space as $\mathcal{H}(\Omega)$ but with homogeneous essential BC and homogeneous GC. For simplicity, we assumed homogeneous natural BC in Eq. (10).

C. The h - ϕ -formulation in helicoidal coordinates

As shown in [31], [32], in order to express the h - ϕ -formulation Eq. (10) in helicoidal coordinates, it is sufficient to replace the scalar material parameters μ and ρ by the tensors $\tilde{\mu}$ and $\tilde{\rho}$:

$$\tilde{\mu} = \mu \mathbf{J}^{-1} \mathbf{J}^{-T} \det(\mathbf{J}) = \mu \mathbf{T}^{-1}, \quad (11)$$

$$\tilde{\rho} = \rho \frac{1}{\det(\mathbf{J})} \mathbf{J}^T \mathbf{J} = \rho \mathbf{T}, \quad (12)$$

with the auxiliary tensor \mathbf{T} , defined by

$$\mathbf{T} = \frac{\mathbf{J}^T \mathbf{J}}{\det(\mathbf{J})} = \begin{pmatrix} 1 & 0 & -\alpha \xi_2 \\ 0 & 1 & \alpha \xi_1 \\ -\alpha \xi_2 & \alpha \xi_1 & 1 + \alpha^2(\xi_1^2 + \xi_2^2) \end{pmatrix}, \quad (13)$$

and its inverse \mathbf{T}^{-1} by

$$\begin{aligned} \mathbf{T}^{-1} &= \det(\mathbf{J}) \mathbf{J}^{-1} \mathbf{J}^{-T} \\ &= \begin{pmatrix} 1 + \alpha^2 \xi_2^2 & \alpha^2 \xi_1 \xi_2 & \alpha \xi_2 \\ \alpha^2 \xi_1 \xi_2 & 1 + \alpha^2 \xi_1^2 & -\alpha \xi_1 \\ \alpha \xi_2 & -\alpha \xi_1 & 1 \end{pmatrix}. \end{aligned} \quad (14)$$

This is a consequence of substituting Eqn. (5) and (6) into Eq. (10) and adding a $\det \mathbf{J}$ factor in the volume integral terms. Beyond these modifications, all calculations can be performed exactly as in Cartesian coordinates [32].

The components of the curl operator in helicoidal coordinates are given by

$$(\mathbf{curl} \mathbf{h})_{\xi} = \begin{pmatrix} \partial_{\xi_2} h_{\xi_3} - \partial_{\xi_3} h_{\xi_2} \\ \partial_{\xi_3} h_{\xi_1} - \partial_{\xi_1} h_{\xi_3} \\ \partial_{\xi_1} h_{\xi_2} - \partial_{\xi_2} h_{\xi_1} \end{pmatrix}. \quad (15)$$

They have the same expression as in Cartesian coordinates, but in terms of the helicoidal coordinates.

D. Conditions for reducing the dimension from 3D to 2D

In the continuous setting, the problems expressed with Cartesian or helicoidal coordinates are equivalent. Indeed, no approximation is introduced and the change of coordinates is regular. For helicoidally symmetric geometries, there are however clear advantages in working with helicoidal coordinates.

First, it involves integrals over domains with ξ_3 -independent sections.

Second, \mathbf{T} and \mathbf{T}^{-1} are also ξ_3 -independent, as shown in Eqn. (13) and (14). As a consequence, both the integrand coefficients and the domains of integration in the weak formulation are ξ_3 -independent.

Finally, if the BC on Γ_{out} are also ξ_3 -independent when expressed in helicoidal coordinates, then, the solution \mathbf{h} of the h - ϕ -formulation is ξ_3 -independent as well. Hence, the integration along the ξ_3 -direction is trivial and the problem dimension

can be reduced from 3D to 2D with a considerable decrease of the computational burden compared to the equivalent 3D problem.

BC are helicoidally symmetric (HS) in the case of a uniform axial magnetic field excitation. In Section III, we describe how the associated 2D problem can be discretized and implemented. We verify the implementation in Section IV.

By contrast, a transverse magnetic field excitation, i.e., a magnetic field in the x - y -plane in the Cartesian coordinate system, does not transform into a ξ_3 -independent field in helicoidal coordinates (see Eq. (25)). In this case, the dimension cannot be *directly* reduced from 3D to 2D. However, simplifications are still possible, eventually also leading to a 2D problem in some situations. We present a novel method for such a situation in Sections V and VI. This method generalizes the case of HS BC, which just becomes a particular case of the general approach.

III. PRACTICAL IMPLEMENTATION OF A FULL h - ϕ -FORMULATION — HS-BC

Starting from Eq. (10) with material tensors in Eqn. (11), one could be tempted to implement the h - ϕ -formulation directly as a classical 2D problem with in-plane magnetic field, with the only differences of (i) working in helicoidal coordinates, and (ii) having anisotropic tensors instead of scalar material parameters. But this would not be correct: the fact that the problem is ξ_3 -independent does not imply that the involved magnetic field has only two non-zero (helicoidal or Cartesian) components.

Due to the full anisotropy of tensors $\tilde{\boldsymbol{\mu}}$ and $\tilde{\boldsymbol{\rho}}$, one really has to consider three independent components for the magnetic field \mathbf{h} in the h - ϕ -formulation. To emphasize this, we refer to the resulting formulation as a *full* h - ϕ -formulation in 2D, and we call the associated model the *2D- ξ model*.

In this section, we present a practical implementation of this full h - ϕ -formulation. First, we propose a convenient decomposition of the magnetic field, which allows us to reuse the usual function spaces of classical 2D problems. Then, we discuss the discretization of these function spaces. Finally, we explain how to impose the GC and BC.

A. Decomposition of the magnetic field

In the h - ϕ -formulation, the magnetic field \mathbf{h} can be decomposed into two parts: an *in-plane* contribution \mathbf{h}_{\parallel} , containing the ξ_1 and ξ_2 -components of \mathbf{h} , and an *out-of-plane* contribution \mathbf{h}_{\perp} , containing only the ξ_3 -component. We write

$$\mathbf{h}(\xi_1, \xi_2) = \mathbf{h}_{\parallel}(\xi_1, \xi_2) + \mathbf{h}_{\perp}(\xi_1, \xi_2), \quad (16)$$

or, explicitly in terms of their helicoidal components,

$$\begin{pmatrix} h_{\xi_1}(\xi_1, \xi_2) \\ h_{\xi_2}(\xi_1, \xi_2) \\ h_{\xi_3}(\xi_1, \xi_2) \end{pmatrix} = \begin{pmatrix} h_{\xi_1}(\xi_1, \xi_2) \\ h_{\xi_2}(\xi_1, \xi_2) \\ 0 \end{pmatrix} + \begin{pmatrix} 0 \\ 0 \\ h_{\xi_3}(\xi_1, \xi_2) \end{pmatrix}, \quad (17)$$

where $\mathbf{h} = \mathbf{h}(\xi_1, \xi_2)$ because the solution is ξ_3 -independent. Note that the vectors \mathbf{h}_{\parallel} and \mathbf{h}_{\perp} are not orthogonal.

Because the Jacobian is non-singular, the curl-free condition Eq. (8) reads, in the helicoidal coordinate system:

$$(\mathbf{curl} \mathbf{h})_{\xi} = \begin{pmatrix} \partial_{\xi_2} h_{\xi_3} \\ -\partial_{\xi_1} h_{\xi_3} \\ \partial_{\xi_1} h_{\xi_2} - \partial_{\xi_2} h_{\xi_1} \end{pmatrix} = \mathbf{0}, \quad (18)$$

from Eq (15) using $\partial_{\xi_3} = 0$. With the decomposition defined in Eq. (16), the third component of Eq. (18) implies that $\mathbf{curl} \mathbf{h}_{\parallel} = \mathbf{0}$, which is the same condition as for a classical 2D formulation in which a two-component magnetic field is considered. Then, for the first two components of Eq. (18) to be equal to zero, the out-of-plane magnetic field \mathbf{h}_{\perp} must be uniform in Ω_c^C .

These conditions are introduced in the function space definitions, i.e., they are strongly enforced. They will be made explicit at the space discretization step.

With the explicit decomposition $\mathbf{h} = \mathbf{h}_{\parallel} + \mathbf{h}_{\perp}$, the h - ϕ -formulation reads as follows. From an initial solution at time $t = 0$, find $\mathbf{h}_{\parallel} \in \mathcal{H}_{\parallel}(\Omega)$ and $\mathbf{h}_{\perp} \in \mathcal{H}_{\perp}(\Omega)$ such that, for $t > 0$, $\forall \mathbf{h}'_{\parallel} \in \mathcal{H}_{\parallel,0}(\Omega)$ and $\forall \mathbf{h}'_{\perp} \in \mathcal{H}_{\perp,0}(\Omega)$,

$$\begin{aligned} \left(\partial_t(\tilde{\boldsymbol{\mu}}(\mathbf{h}_{\parallel} + \mathbf{h}_{\perp})), \mathbf{h}'_{\parallel} \right)_{\Omega} + \left(\tilde{\boldsymbol{\rho}} \mathbf{curl}(\mathbf{h}_{\parallel} + \mathbf{h}_{\perp}), \mathbf{curl} \mathbf{h}'_{\parallel} \right)_{\Omega_c} \\ = \sum_{i \in C_V} \bar{V}_i \mathcal{I}_i(\mathbf{h}'_{\parallel}), \end{aligned} \quad (19)$$

$$\begin{aligned} \left(\partial_t(\tilde{\boldsymbol{\mu}}(\mathbf{h}_{\parallel} + \mathbf{h}_{\perp})), \mathbf{h}'_{\perp} \right)_{\Omega} + \left(\tilde{\boldsymbol{\rho}} \mathbf{curl}(\mathbf{h}_{\parallel} + \mathbf{h}_{\perp}), \mathbf{curl} \mathbf{h}'_{\perp} \right)_{\Omega_c} \\ = 0, \end{aligned} \quad (20)$$

where the vectors \mathbf{h}_{\parallel} and \mathbf{h}_{\perp} are coupled by tensors $\tilde{\boldsymbol{\mu}}$ and $\tilde{\boldsymbol{\rho}}$. Note that $\mathcal{I}_i(\mathbf{h}'_{\perp}) = 0$. The function spaces $\mathcal{H}_{\parallel}(\Omega)$ and $\mathcal{H}_{\perp}(\Omega)$ will be defined in the space discretization step.

For the resistivity in superconducting materials, the power law Eq. (9) leads to $\tilde{\boldsymbol{\rho}} = \rho_{SC}(\|\mathbf{j}\|) \mathbf{T}$. Using Eq. (6) and $\det \mathbf{J} = 1$, we have, in terms of the components: $\|\mathbf{j}\|^2 = \mathbf{j}_x^T \mathbf{j}_x = \mathbf{j}_{\xi}^T \mathbf{J}^T \mathbf{J} \mathbf{j}_{\xi} = \mathbf{j}_{\xi}^T \mathbf{T} \mathbf{j}_{\xi}$, which is ξ_3 -independent.

B. Space discretization of the magnetic field

Let us consider a finite element mesh for the discretization of the 2D domain Ω , and let us denote by $\mathcal{N}(\Omega_i)$ and $\mathcal{E}(\Omega_i)$, the set of nodes and edges, respectively, of the mesh in a given (sub-)domain Ω_i , including entities on the boundary of Ω_i .

In practice, we can discretize the in-plane magnetic field \mathbf{h}_{\parallel} exactly as the two-component magnetic field in a classical 2D h - ϕ -formulation with in-plane magnetic field [23]. We use Whitney forms [33]: gradient of node functions w_n and cohomology functions \mathbf{c}_i (cut functions) [34] in Ω_c^C , and edge functions \mathbf{w}_e in $\Omega_c \setminus \partial\Omega_c$:

$$\mathbf{h}_{\parallel} = \sum_{e \in \mathcal{E}(\Omega_c \setminus \partial\Omega_c)} h_{\parallel,e} \mathbf{w}_e + \sum_{n \in \mathcal{N}(\Omega_c^C)} \phi_n \mathbf{grad} w_n + \sum_{i \in C} I_i \mathbf{c}_i, \quad (21)$$

where coefficients $h_{\parallel,e}$, ϕ_n , and I_i are the degrees of freedom (DOFs) defining \mathbf{h}_{\parallel} in the discrete function space $\mathcal{H}_{\parallel}(\Omega)$.

We choose to discretize the out-of-plane magnetic field \mathbf{h}_{\perp} with perpendicular edge functions $\mathbf{w}_n = w_n \hat{\boldsymbol{e}}_{\xi_3}$, associated with nodes. To account for the fact that \mathbf{h}_{\perp} must be uniform in each region of Ω_c^C , we introduce global functions in Ω_c^C . Let

K be the number of connected regions in Ω_c^C . We describe the out-of-plane magnetic field with the expansion

$$\mathbf{h}_\perp = \sum_{n \in \mathcal{N}(\Omega_c \setminus \partial\Omega_c)} h_{\perp,n} \mathbf{w}_n + \sum_{i=1}^K D_i \mathbf{p}_i, \quad (22)$$

with \mathbf{w}_n the perpendicular edge function associated with node n in $\mathcal{N}(\Omega_c \setminus \partial\Omega_c)$, and \mathbf{p}_i a global shape function defined as the sum of all perpendicular edge functions associated with nodes in the i^{th} connected region of Ω_c^C , including those on its boundary, for $i \in \{1, \dots, K\}$. The support of the shape function \mathbf{p}_i is therefore not restricted to Ω_c^C : it is non-zero on a layer of one element adjacent to $\partial\Omega_c$ in Ω_c . This defines the discrete function space $\mathcal{H}_\perp(\Omega)$, with DOFs $h_{\perp,n}$ and D_i . Both \mathbf{h}_\parallel and \mathbf{h}_\perp are described by discrete 1-forms, and so is their sum, \mathbf{h} .

For simplicity, in the following, we assume that there is only one connected non-conducting region Ω_c^C , the exterior of the wire, such that $K = 1$, and we rename $D_1 = D$.

C. Global conditions and boundary conditions

For the GC, a current \bar{I}_i , for $i \in C_I$, can be imposed exactly as in a classical 2D h - ϕ -formulation with in-plane magnetic field, i.e., strongly via the degree of freedom I_i associated with the cut function \mathbf{c}_i for the corresponding conducting domain Ω_{c_i} . Alternatively, an applied voltage \bar{V}_i , for $i \in C_V$, can be imposed weakly in the global term of the formulation Eq. (19).

For the BC, we consider a circular external boundary Γ_{out} , placed in Ω_c^C sufficiently far from the conductors such that we can assume $\partial_t \mathbf{b} \cdot \mathbf{n}|_{\Gamma_{\text{out}}} = 0$, with \mathbf{n} the outer normal vector. This condition is implicitly imposed for \mathbf{h}_\parallel in Eq. (19) with homogeneous natural BC on Γ_{out} . This lets the z -component of the magnetic field, h_z , undetermined on Γ_{out} . It corresponds to the axial magnetic field, that we can freely impose. We derive below how to translate this into a BC on $\mathbf{h}_\perp|_{\Gamma_{\text{out}}}$ in helicoidal coordinates.

Let us first consider the situation with a zero axial magnetic field. At a sufficiently large distance R_{out} from the center of conductors carrying a total net current intensity I , the magnetic field tends to be purely azimuthal and axisymmetric. We have $\mathbf{h}_\mathbf{x} = \frac{I}{2\pi R_{\text{out}}} (-\sin\theta \ \cos\theta \ 0)^T$, with $\theta = \text{atan2}(y, x)$. In terms of the helicoidal coordinates, on the plane $\xi_3 = 0$, it reads

$$\begin{aligned} \mathbf{h}_\xi = \mathbf{J}^T|_{\xi_3=0} \mathbf{h}_\mathbf{x} &= \frac{I}{2\pi R_{\text{out}}} \begin{pmatrix} -\sin\theta \\ \cos\theta \\ \alpha\xi_2 \sin\theta + \alpha\xi_1 \cos\theta \end{pmatrix} \\ &= \frac{I}{2\pi R_{\text{out}}} \begin{pmatrix} -\sin\theta \\ \cos\theta \\ \alpha R_{\text{out}} \end{pmatrix}, \end{aligned} \quad (23)$$

using $\xi_2 = R_{\text{out}} \sin\theta$ and $\xi_1 = R_{\text{out}} \cos\theta$ for $\xi_3 = 0$. Consequently, to satisfy $h_z|_{\Gamma_{\text{out}}} = 0$, one has to impose that $h_{\xi_3}|_{\Gamma_{\text{out}}} = I\alpha/2\pi$. This can be done by fixing the degree of freedom D associated with the basis function \mathbf{p} in Ω_c^C in Eq. (22) to the value $D = I\alpha/2\pi$. Note that this value does not depend on R_{out} .

By superposition, if one wants to impose a non-zero axial magnetic field h_{axial} on the external boundary Γ_{out} in addition

to a net current intensity I , we can impose the following condition:

$$D = \frac{I\alpha}{2\pi} + h_{\text{axial}}, \quad (24)$$

because the axial magnetic field Cartesian components $\mathbf{h}_\mathbf{x} = (0 \ 0 \ h_{\text{axial}})^T$ transform into $\mathbf{h}_\xi = \mathbf{J}^T \mathbf{h}_\mathbf{x} = (0 \ 0 \ h_{\text{axial}})^T$ in helicoidal coordinates.

IV. VERIFICATION AND APPLICATION — HS-BC

In this section, we first compare the solution of the 2D- ξ model in helicoidal coordinates to the solution of a classical 3D h - ϕ -formulation on a simple problem in order to verify the implementation. We also quantify the computational gain offered by reducing the dimension from 3D to 2D. Then, we apply the 2D- ξ model on a more involved geometry to illustrate the capabilities of the approach.

A. Verification problem

We consider a wire made of six identical Nb-Ti superconducting filaments, twisted and embedded in a copper (Cu) matrix, as illustrated in Fig. 3. In order to simplify the geometry, the cross sections of the filaments are assumed to be disks, and the 3D geometry is generated by a helicoidal extrusion of them. This is of course an approximation of a realistic geometry. If needed, cross sections of round twisted filaments can be computed accurately using envelope theory as in [15] or CAD tools [25] as in [17].

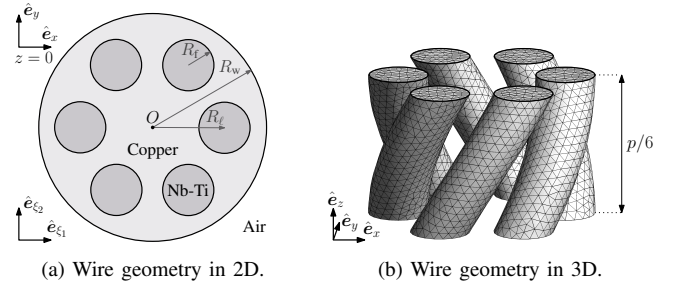


Fig. 3: Wire geometry for the verification of the helicoidal transformation consisting of six twisted Nb-Ti filaments embedded in a copper matrix. (a) Geometry in a ξ_1 - ξ_2 plane (or in the x - y plane for $z = 0$). (b) One-sixth of a pitch length. The copper matrix in (b) is not represented, for clarity.

The filaments have a radius of $R_f = 35 \ \mu\text{m}$ and their centers are at a distance $R_\ell = 98 \ \mu\text{m}$ from the center of the wire. The wire has a radius of $R_w = 155 \ \mu\text{m}$ and a pitch length of $p = 1 \ \text{mm}$. The air is modelled outside of the wire up to a distance $R_{\text{out}} = 500 \ \mu\text{m}$.

We assume that Nb-Ti resistivity is characterized by Eq. (9) with constant and uniform $j_c = 7 \times 10^9 \ \text{A/m}^2$ and $n = 50$, and that the copper resistivity is $\rho_{\text{Cu}} = 1.81 \times 10^{-10} \ \Omega\text{m}$. There is no insulation between the filaments and the matrix, so that the wire behaves as a single conducting cylinder. A net transport current $I(t) = 0.5 I_c \sin(2\pi t/T)$ is imposed in the wire, with $T = 0.1 \ \text{s}$ and $I_c = 162 \ \text{A}$, and we impose $h_{\text{axial}} = 0 \ \text{A/m}$.

B. Implementation of the 3D model

We consider the 3D geometry represented in Fig. 3(b). It represents a periodic cell of one-sixth of a whole pitch length p . Note that building and meshing the 3D model represented in Fig. 3(b) is not a trivial task. To account for the periodicity of the problem, the mesh must be identical on the top and bottom boundaries of the domain; as an h - ϕ -formulation is used, cohomology basis functions must also be periodic. The quality of the mesh inside the filaments plays an important role for the accuracy of the resulting numerical solution. We observed that better results are obtained with a structured mesh inside the filaments. Generating the mesh with such constraints is possible with Gmsh [25]. The periodic support for the cohomology basis function is generated as described in [34], [35] and illustrated in Fig. 4.

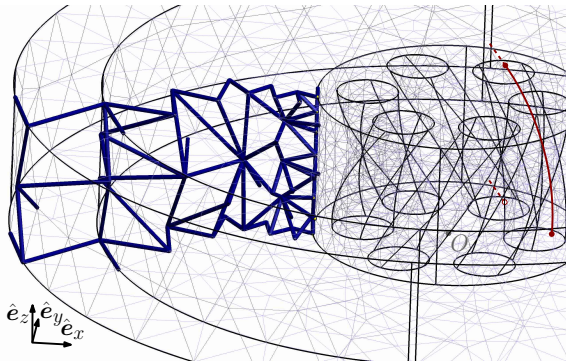


Fig. 4: Periodic support for the cohomology basis function to impose a transport current $I(t)$ in the 3D verification model. The red curve in the filaments is a portion of the helical fiber along which the solution is represented in Fig. 5.

We set a homogeneous natural BC on the external boundary Γ_{out} , so that $\partial_t \mathbf{b} \cdot \mathbf{n}|_{\Gamma_{\text{out}}} = 0$ is weakly enforced. For the top and bottom boundaries Γ_{up} and Γ_{down} , which are topologically identical, the periodic condition $\mathbf{h} \times \mathbf{n}|_{\Gamma_{\text{up}}} = -\mathbf{h} \times \mathbf{n}|_{\Gamma_{\text{down}}}$ is imposed. On conducting boundaries $\partial\Omega_c \cap (\Gamma_{\text{up}} \cup \Gamma_{\text{down}})$, this is done by forcing the equality of the degrees of freedom associated with topologically identical edges of these boundaries. On non-conducting boundaries $\partial\Omega_c^c \cap (\Gamma_{\text{up}} \cup \Gamma_{\text{down}})$, the periodic constraint is enforced via the magnetic scalar potential. We impose $\phi|_{\Gamma_{\text{up}}} = \phi|_{\Gamma_{\text{down}}} + h_{\text{axial}} p/6$. The total current intensity flowing in the conducting domain made up of the filaments and matrix is imposed via the (periodic) cohomology basis function whose generating edges are highlighted in Fig. 4.

Note that in the present case of HS-BC (transport current or axial field), the 3D reference model could be defined on a length shorter than $p/6$ along z , if one adapts the periodic mesh and the periodic cut accordingly. We chose a length of $p/6$ so that the reference model will also be valid in the transverse field case.

Before comparing the results, we first verify that the 3D model indeed produces a helicoidally symmetric solution. For illustration, from the 3D numerical solution, we extract the magnetic field \mathbf{h} and the current density \mathbf{j} along the helical fiber of pitch length p passing at point $\mathbf{x} = (a, b, 0)$, with $a = 180$ mm and $b = 11$ mm, from $z = 0$ to $z = p$ (see Fig. 4). We exploit the periodicity of the problem to obtain values for $z >$

$p/6$. The Cartesian and helicoidal components of vectors \mathbf{h} and \mathbf{j} are represented in Fig. 5 for a relatively fine tetrahedral mesh (144 870 DOFs), at time $t = T/4$. Helicoidal components are obtained using the one and two-forms transformation relations, Eqn. (5) and (6).

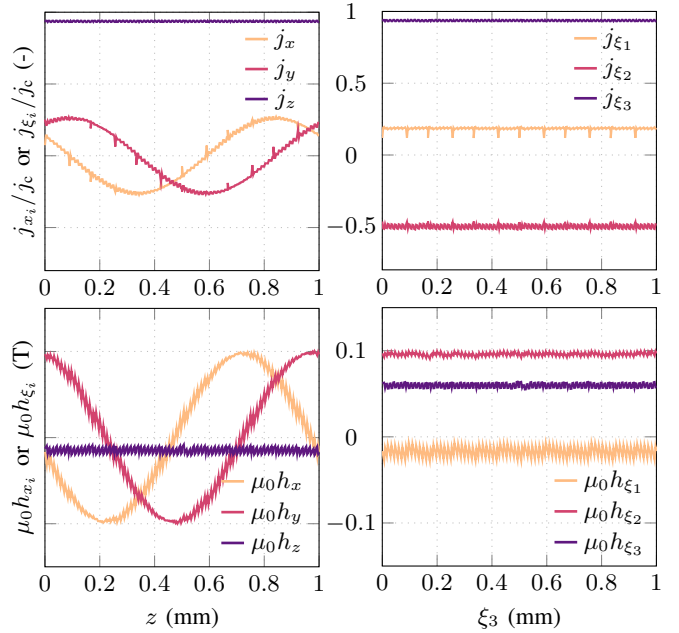


Fig. 5: Current density (up) and magnetic field (down) components along a helical fiber from $z = 0$ to $z = p$. (Left) Cartesian components of the vectors. (Right) Helicoidal components of the vectors. Solution at $t = T/4$.

The oscillations and spikes along the fiber represent inter-element non-conformities, which are expected with lowest-order tetrahedral Whitney shape functions. These oscillations decrease in amplitude with mesh refinement. Up to these inter-element variations, the 3D solution correctly presents a helicoidal symmetry. It is also interesting to notice that the current density has non-zero ξ_1 and ξ_2 -components, and that the ξ_3 -component of the magnetic field is not equal to zero. This illustrates the need for a three-component magnetic field in the 2D helicoidal model.

C. Comparison of the results from the 3D and 2D- ξ models

We now compare the results of the 2D- ξ problem in helicoidal coordinates with the reference 3D problem described above. Note that for the 2D- ξ model, in this particular case, we could further exploit the symmetry and model only one-sixth of the circular region depicted in Fig. 3(a) using periodic BC on the symmetry boundaries as well as an adapted cohomology function in Ω_c^c , hence reducing the computational cost even more. We however choose to model the full 2D cross section.

The solution of the 2D- ξ model on a medium mesh resolution (4700 DOFs) is represented in Fig. 6. The current mostly flows in the superconducting filaments, as shown by the different scales for the middle and right subfigures. On the left subfigure, one can see that the current flow in the twisted filaments induces a non-zero z -component h_z of the magnetic field at the center of the wire.

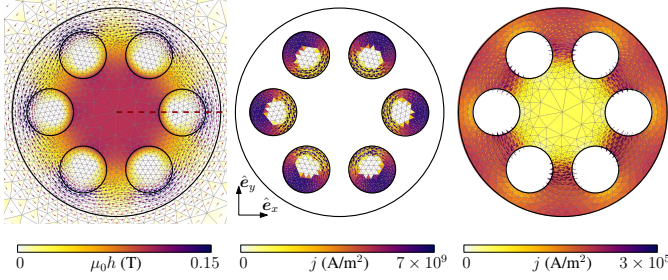


Fig. 6: Magnetic field (left), current density in the filaments (middle), and current density in the matrix (right) at time $t = T/4$ for the 2D- ξ problem solved with the helicoidal coordinate system. The arrows represent the in-plane x and y -components of \mathbf{h} and \mathbf{j} , whereas the triangular elements are colored as a function of the out-of-plane z -component of \mathbf{h} and \mathbf{j} . The dashed red line in the left figure is the cut along which the magnetic field is represented in Fig. 7.

A comparison of the local magnetic field of the 2D- ξ model with that of the reference 3D model is given in Fig. 7, along the dashed red line highlighted in Fig. 6, for two mesh resolutions. The solution of the 3D model is taken on the plane $z = \xi_3 = 0$, but this choice is arbitrary: as was shown in Fig. 5, up to the inter-element variation, the solution of the 3D model is also ξ_3 -independent. Solutions of the 2D- ξ and 3D models match locally. We verified and this is also the case for the current density (not represented in the figures).

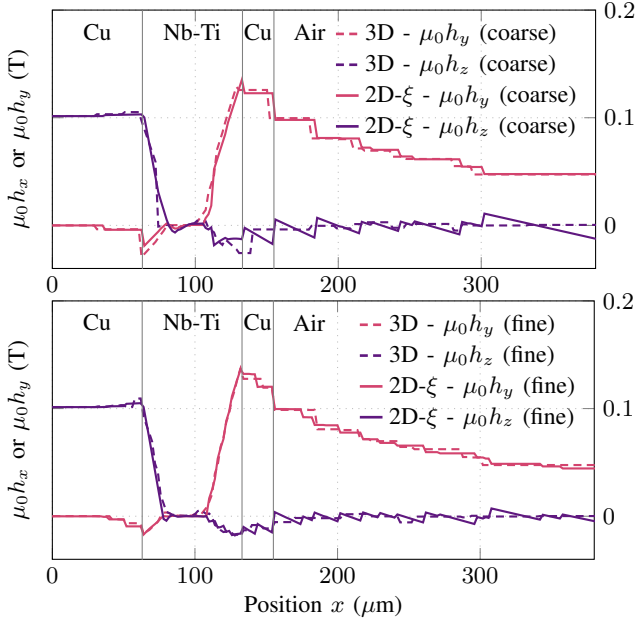


Fig. 7: Magnetic field along the dashed red line represented in Fig. 6, for the 3D and 2D- ξ models, at time $t = T/4$, with coarse (up) and fine (down) mesh resolutions.

A comparison of the AC loss is given in Fig. 8. The AC loss per unit length along \hat{e}_z in both the superconducting filaments and the conducting matrix are compared for the two models, and for two mesh resolutions. For the 2D- ξ model in helicoidal coordinates, the AC loss is computed as $(\tilde{\rho} \mathbf{j}_\xi, \mathbf{j}_\xi)_{\Omega_c}$, where Ω_c is either restricted to the filaments, or to the matrix. For the 3D model, the integral $(\rho \mathbf{j}_x, \mathbf{j}_x)_{\Omega_c}$ is computed over the

3D domain with Cartesian coordinate system, and the result is divided by $p/6$, to obtain the AC loss per unit length as well. Note that both models include all loss contributions by construction: hysteresis losses in the filaments, as well as coupling and eddy current losses in the matrix [36].

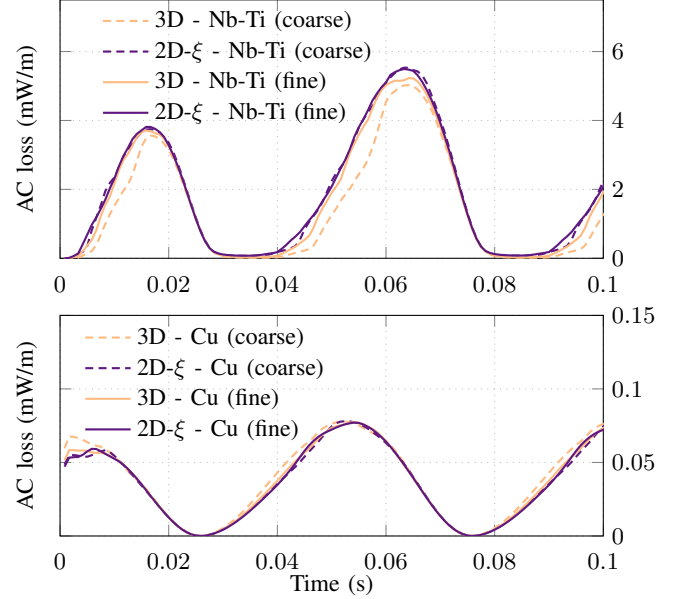


Fig. 8: AC losses in the superconducting filaments (up) and in the conducting matrix (down) for a transport current $I(t)$, as a function of time, for two mesh resolutions, with the 2D- ξ model in helicoidal coordinates and the 3D verification model.

Meshes for the coarse resolution in the $z = \xi_3 = 0$ plane are similar for the 2D- ξ and 3D models, as well as meshes for the fine resolution. However, we observed that the 2D- ξ model solution is less sensitive to the mesh resolution. This is due to the inter-element non-conformities in a tetrahedral 3D mesh, which should be made significantly lower (by mesh refinement) to ensure an accurate evaluation of the quadratic quantity representing the AC losses. Meshes with prisms, i.e., extruded triangles, in the filaments were also tested. They give slightly better results, but also increase the complexity of the meshing step, as pyramids must be used as transition elements between prisms in the filaments and tetrahedra outside of them.

The local and global quantity agreement shows the validity of the 2D- ξ model in helicoidal coordinates. The dimension reduction allows for a very large reduction of the computational cost. This is demonstrated in Table I, which compares the performance of the 2D- ξ and 3D models on meshes with similar characteristic length for the finite elements (triangles in 2D- ξ and tetrahedra in 3D). The fine 2D- ξ model is more than two orders of magnitude faster to solve than the fine 3D model.

D. Application to a 54-filament wire

As a more realistic geometry, we consider a wire with 54 filaments arranged in a hexagonal lattice with filament center spacing of $d = 110 \mu\text{m}$, as represented in Fig. 9. Filament radius is $R_f = 45 \mu\text{m}$, wire radius is $R_w = 500 \mu\text{m}$, and

Model & mesh	# DOFs	# it.	Time/it./DOF	Total time	
3D	Coarse	16 556	1 645	110 μ s	50 m
	Medium	85 605	2 893	260 μ s	17 h 53 m
	Fine	144 870	3 255	315 μ s	41 h 23 m
2D- ξ	Coarse	1 797	1 299	72 μ s	3 m
	Medium	4 481	1 948	71 μ s	10 m
	Fine	6 002	2 258	76 μ s	17 m

TABLE I: Performance comparison for the 3D and 2D- ξ models with imposed current and no axial magnetic field, computed with 150 time steps from $t = 0$ to $t = 5T/4$ on a single Intel Core i7 2.2 GHz CPU. DOF: degree of freedom. It.: iteration (Newton-Raphson).

the pitch length is $p = 10$ mm. We keep the same material parameters as before for the Nb-Ti and the copper matrix and we impose a transport current $I(t) = 0.8 I_c \sin(2\pi t/T)$, with $T = 1$ s and $I_c = 2.4$ kA.

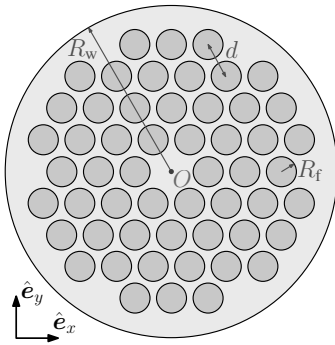


Fig. 9: Cross section of the 54-filament Nb-Ti/Cu wire.

Fig. 10 shows the time evolution of the current in the filaments depending on their position. As expected, the current density progressively penetrates into inner layers of the wire. Due to the twist, the current flowing in the outer filaments generates a non-zero h_z component inside the wire. Circulating in-plane currents therefore appear in the inner layers to shield this axial magnetic field, as illustrated in Fig. 11.

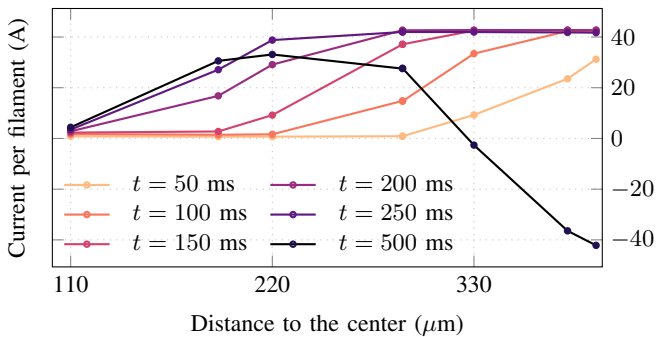


Fig. 10: Distribution of the current among the filaments, as a function of their distance to the center O , for the 54-filament geometry.

Note that during the first transport current increase (for $t < T/4$), no filament carries a negative current. This is in contradiction to what was obtained in [37] with an alternative method on a similar problem, where a critical state model is considered and the current density is assumed localized along a line within every filament, which therefore leads to neglecting the spatial extension of the filaments.

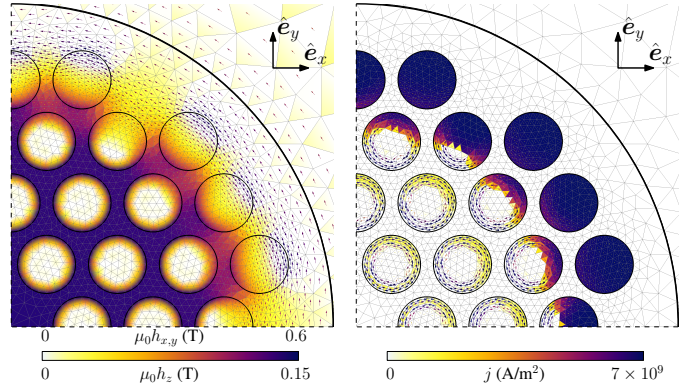


Fig. 11: Magnetic field (left) and current density (right) for the 54-filament wire at time $t = 0.1$ s. Only one quarter of the geometry is shown. Arrows represent the in-plane components and the elements are colored as a function of the value of the z -component of the vectors. Note that two different scales are used for the magnetic field for clarity.

V. EXTENSION TO NON-HELICOIDALLY-INVARIANT BOUNDARY CONDITIONS — GENERAL BC

When BC are not HS, the dimension of the problem cannot be directly reduced from 3D to 2D on basis of the geometrical symmetry only. This is the case when a wire is subjected to a uniform transverse magnetic field. For an applied magnetic field $\mathbf{h}_x = (0 \ 1 \ 0)^T$, we have

$$\mathbf{h}_\xi = \mathbf{J}^T \mathbf{h}_x = \begin{pmatrix} \sin \alpha \xi_3 \\ \cos \alpha \xi_3 \\ \alpha \xi_1 \cos \alpha \xi_3 - \alpha \xi_2 \sin \alpha \xi_3 \end{pmatrix}, \quad (25)$$

which is not ξ_3 -independent, see Fig. 12. As a consequence, the solution of the magnetodynamic problem will not be ξ_3 -independent either. The periodic structure of the problem can however be exploited by expressing the solution as a series of periodic functions with respect to ξ_3 .

In this section, we present this approach and show that it generalizes the method described in Section III. In particular, we show that it also leads to a 2D model in helicoidal coordinates, which has the potential of considerably reducing the computational cost compared to a 3D model.

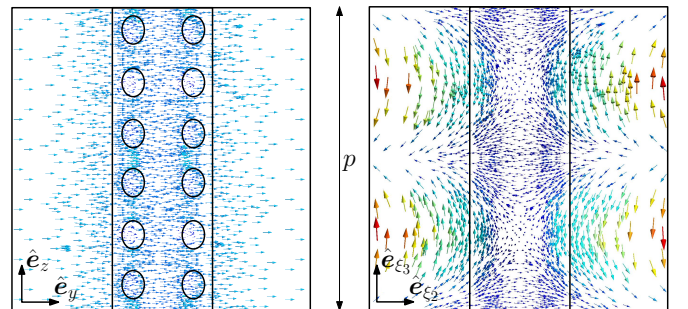


Fig. 12: Uniform magnetic field along \hat{e}_y for the six-filament geometry represented in Fig. 3. (Left) In the physical space on the plane $x = 0$. (Right) In the helicoidal coordinate system represented as an orthogonal system on the plane $\xi_1 = 0$.

A. Fourier decomposition of the magnetic field

Given the p -periodicity with respect to ξ_3 , by separation of variables, we can expand the magnetic field $\mathbf{h} = \mathbf{h}(\xi_1, \xi_2, \xi_3)$ in the following series:

$$\mathbf{h}(\xi_1, \xi_2, \xi_3) = \sum_{k=-\infty}^{\infty} \mathbf{h}_k(\xi_1, \xi_2) f_k(\xi_3), \quad (26)$$

with the *modes* $f_k = f_k(\xi_3)$ that are functions of ξ_3 only and that are defined as

$$f_k(\xi_3) = \begin{cases} \sqrt{2} \cos(\alpha k \xi_3), & k < 0, \\ 1, & k = 0, \\ \sqrt{2} \sin(\alpha k \xi_3), & k > 0, \end{cases} \quad (27)$$

and with the *spatial Fourier coefficients* $\mathbf{h}_k = \mathbf{h}_k(\xi_1, \xi_2)$ that are three-component vector functions of ξ_1 and ξ_2 .

The modes f_k are mutually orthogonal and have a unit norm, denoted as $\|f_k\| = 1$, in the sense of the following inner product:

$$\langle f_{k_1}, f_{k_2} \rangle = \frac{1}{p} \int_0^p f_{k_1} f_{k_2} d\xi_3 = \delta_{k_1 k_2}, \quad \forall k_1, k_2 \in \mathbb{Z}. \quad (28)$$

They also satisfy the following property:

$$\frac{df_k}{d\xi_3} = \alpha k f_{-k}, \quad \forall k \in \mathbb{Z}. \quad (29)$$

Introducing a decomposition of the magnetic field into its in-plane and out-of-plane components as in the HS case of Section III for each Fourier coefficient \mathbf{h}_k , we can rewrite Eq. (26) as

$$\mathbf{h} = \sum_{k=-\infty}^{\infty} (\mathbf{h}_{\parallel, k}(\xi_1, \xi_2) + \mathbf{h}_{\perp, k}(\xi_1, \xi_2)) f_k(\xi_3), \quad (30)$$

with the $\mathbf{h}_{\parallel, k}$ containing the ξ_1 and ξ_2 -components of \mathbf{h}_k , and the $\mathbf{h}_{\perp, k}$ containing its ξ_3 -component. Equation (30) actually generalizes the decomposition in Eq. (16) for the case of HS BC. Indeed, in the case of HS BC, the only mode that is involved is $f_0(\xi_3) = 1$, with coefficients $\mathbf{h}_{\parallel, 0} = \mathbf{h}_{\parallel}$ and $\mathbf{h}_{\perp, 0} = \mathbf{h}_{\perp}$, and the coefficients of the other modes, $\mathbf{h}_{\parallel, k}$ and $\mathbf{h}_{\perp, k}$, $\forall k \in \mathbb{Z}_0$, are all equal to zero.

B. Space discretization with curl-free functions in Ω_c^C

The curl of decomposition (30) reads

$$\mathbf{curl} \mathbf{h} = \sum_{k=-\infty}^{\infty} \left(f_k \mathbf{curl} \mathbf{h}_{\parallel, k} + \frac{df_k}{d\xi_3} \hat{\mathbf{e}}_{\xi_3} \times \mathbf{h}_{\parallel, k} + f_k \mathbf{curl} \mathbf{h}_{\perp, k} \right), \quad (31)$$

where $\hat{\mathbf{e}}_{\xi_3}$ is the unit vector in the ξ_3 -direction.

The only term in Eq. (31) contributing to the ξ_3 -component of the curl involves the curl of $\mathbf{h}_{\parallel, k}$. We can therefore keep the same discrete function space for the $\mathbf{h}_{\parallel, k}$ as for \mathbf{h}_{\parallel} in Section III, however without the $\sum_i I_i \mathbf{c}_i$ term of Eq. (21) for $k \neq 0$, as transport currents only contribute to the fundamental mode with $f_0(\xi_3) = 1$.

As in the ξ_3 -independent case, we express the out-of-plane magnetic field $\mathbf{h}_{\perp, k}$ as a sum of perpendicular edge functions.

But now, the $\mathbf{h}_{\parallel, k}$ functions also contribute to the ξ_1 and ξ_2 -components of the curl of \mathbf{h} for $k \neq 0$ in Eq. (31) via the cross product term. Therefore, the curl-free condition in Ω_c^C is no longer met with a uniform out-of-plane magnetic field in Ω_c^C , for $k \neq 0$. Instead, as is shown below, the curl-free condition induces a coupling between the in-plane and out-of-plane magnetic field contributions in Ω_c^C . For simplicity, as was done before, we assume that there is only one connected non-conducting region Ω_c^C .

Using curl-free in-plane functions $\mathbf{h}_{\parallel, k}$ in Ω_c^C and Eq. (31), the curl-free condition on \mathbf{h} in Ω_c^C reads

$$\sum_{k=-\infty}^{\infty} \left(\frac{df_k}{d\xi_3} \hat{\mathbf{e}}_{\xi_3} \times \mathbf{h}_{\parallel, k} + f_k \mathbf{curl} \mathbf{h}_{\perp, k} \right) = \mathbf{0}. \quad (32)$$

Using the mode property Eq. (29), this yields

$$\sum_{k=-\infty}^{\infty} \left(\mathbf{curl} \mathbf{h}_{\perp, k} - \alpha k \hat{\mathbf{e}}_{\xi_3} \times \mathbf{h}_{\parallel, -k} \right) f_k = \mathbf{0}, \quad (33)$$

which results in the following condition, $\forall k \in \mathbb{Z}$:

$$\mathbf{curl} \mathbf{h}_{\perp, k} - \alpha k \hat{\mathbf{e}}_{\xi_3} \times \mathbf{h}_{\parallel, -k} = \mathbf{0}. \quad (34)$$

For $k = 0$, we retrieve the same condition as in the helicoidally symmetric problem, that is, $\mathbf{h}_{\perp, 0}$ must be uniform in Ω_c^C , with a value given by Eq. (24). For $k \neq 0$, the condition can be enforced via the independent degrees of freedom of the in-plane and out-of-plane magnetic field contributions. Indeed, in Ω_c^C , we have the expansions

$$\mathbf{h}_{\perp, k} = \sum_{n \in \mathcal{N}(\Omega_c^C)} h_{\perp, k, n} w_n \hat{\mathbf{e}}_{\xi_3}, \quad (35)$$

$$\mathbf{h}_{\parallel, -k} = \sum_{n \in \mathcal{N}(\Omega_c^C)} \phi_{\parallel, -k, n} \mathbf{grad} w_n, \quad (36)$$

where $w_n \hat{\mathbf{e}}_{\xi_3} = \mathbf{w}_n$ is the perpendicular edge function of node n , with w_n the usual node function. In terms of the individual degrees of freedom, Eq. (34) reads

$$\sum_{n \in \mathcal{N}(\Omega_c^C)} (h_{\perp, k, n} + \alpha k \phi_{\parallel, -k, n}) \begin{pmatrix} \partial_{\xi_2} w_n \\ -\partial_{\xi_1} w_n \\ 0 \end{pmatrix} = \mathbf{0}. \quad (37)$$

This equation is valid over the whole domain Ω_c^C if and only if the first parenthesis is constant. This is the case if, for $k \neq 0$,

$$h_{\perp, k, n} + \alpha k \phi_{\parallel, -k, n} = 0, \quad \forall n \in \mathcal{N}(\Omega_c^C). \quad (38)$$

That is, to ensure a curl-free magnetic field in Ω_c^C , the degrees of freedom of the mode $\mathbf{h}_{\perp, k}$ must be linked directly to those of the mode $\mathbf{h}_{\parallel, -k}$ in Ω_c^C (or vice-versa).

This link between the degrees of freedom strongly ensures that $\mathbf{curl} \mathbf{h} = \mathbf{0}$ in Ω_c^C and allows for a significant reduction of the number of unknowns, hence a reduction of the computational cost of the resolutions.

C. Boundary conditions for a transverse magnetic field

The transverse magnetic field defined in Eq. (25) applied as a BC on Γ_{out} only involves the modes $f_{-1}(\xi_3)$ and $f_1(\xi_3)$. We have, in helicoidal components:

$$(\mathbf{h}_{\parallel,-1})_{\xi} = \frac{\sqrt{2}}{2} (0 \ 1 \ 0)^T, \quad (39)$$

$$(\mathbf{h}_{\perp,-1})_{\xi} = \frac{\sqrt{2}}{2} (0 \ 0 \ \alpha\xi_1)^T, \quad (40)$$

$$(\mathbf{h}_{\parallel,+1})_{\xi} = \frac{\sqrt{2}}{2} (1 \ 0 \ 0)^T, \quad (41)$$

$$(\mathbf{h}_{\perp,+1})_{\xi} = \frac{\sqrt{2}}{2} (0 \ 0 \ -\alpha\xi_2)^T. \quad (42)$$

We can verify that they satisfy Eq. (34).

D. Derivation of the h - ϕ -formulation with linear materials

With linear materials, orthogonality allows solving modes with different values of $|k|$ (i.e., including $-k$ and k) independently. For each value of $|k|$, the integration along ξ_3 gives an independent set of equations, written in terms of the unknown Fourier coefficients $\mathbf{h}_{\parallel,-k}$, $\mathbf{h}_{\perp,-k}$, $\mathbf{h}_{\parallel,k}$, and $\mathbf{h}_{\perp,k}$. These coefficients are functions of ξ_1 and ξ_2 only, and hence the problem is 2D. The formulation is derived in the Appendix.

For nonlinear materials, the modes are no longer decoupled. We provide observations and comments on how to handle this situation in Section VI-C.

VI. VERIFICATION AND APPLICATION — GENERAL BC

In this section, we first verify the implementation of the generalized 2D- ξ method by comparing its results with those of a 3D reference model, for linear materials. We then apply the method on a 54-filament wire and discuss the different contributions to the total AC loss, still with linear materials. Finally, we comment on the application of the method in the case of nonlinear materials.

A. Verification with linear materials

The validity of the approach with linear materials is verified by comparing the results of the 2D- ξ model with those obtained with a classical 3D model. We consider the same geometry as in Section IV, but with a constant resistivity in the filaments, and with a uniform transverse magnetic field instead of an imposed transport current.

The filaments have a constant resistivity $\rho_{\text{SC}} = 3.3 \times 10^{-14}$ Ωm (dummy value chosen for verification), and the matrix has a constant resistivity $\rho_{\text{Cu}} = 1.81 \times 10^{-10}$ Ωm . The system is subjected to a transverse magnetic field along y , increasing from 0 T to 0.1 T with a constant ramp-up rate of 18 T/s.

Boundary conditions for the 2D- ξ model are imposed on Γ_{out} so as to satisfy Eqn. (39) to (42). Only modes $f_{-1}(\xi_3) = \sqrt{2} \cos \alpha\xi_3$ and $f_{+1}(\xi_3) = \sqrt{2} \sin \alpha\xi_3$ are therefore excited so that the full magnetic field reads

$$\mathbf{h} = (\mathbf{h}_{\parallel,-1}(\xi_1, \xi_2) + \mathbf{h}_{\perp,-1}(\xi_1, \xi_2)) f_{-1}(\xi_3) + (\mathbf{h}_{\parallel,+1}(\xi_1, \xi_2) + \mathbf{h}_{\perp,+1}(\xi_1, \xi_2)) f_{+1}(\xi_3). \quad (43)$$

The result of the linear 2D- ξ model is illustrated in Fig. 13.

Comparisons with the solution of the 3D problem are given in Figs. 14 and 15, along a characteristic line in the $z = \xi_3 = 0$ plane and along a helicoidal fiber of pitch length p , passing at point $\mathbf{x} = (r, 0, 0)$, with $r = R_{\ell} + 0.8R_f$, from $z = 0$ to $z = p$. Both models agree with each other.

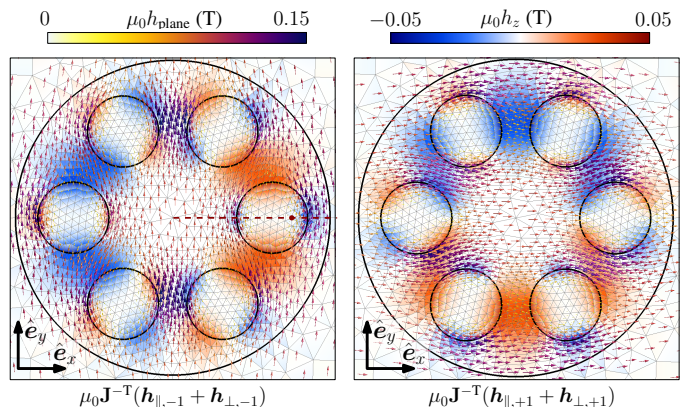


Fig. 13: Solution of the 2D- ξ model with linear materials, on the $z = 0$ plane, for a transverse field of 0.1 T. The arrows represent $\mu_0 \mathbf{h}$, and the triangular elements are colored as a function of the value of $\mu_0 h_z$, using the color map on the top. The dashed red line is where the field is taken for Fig. 14, and the red dot along that line represents the intersection with the plane $z = 0$ of the helicoidal fiber along which the field is taken for Fig. 15. (Left) Mode with $f_{-1}(\xi_3)$ (see Eq. (43)). (Right) Mode with $f_{+1}(\xi_3)$ (see Eq. (43)).

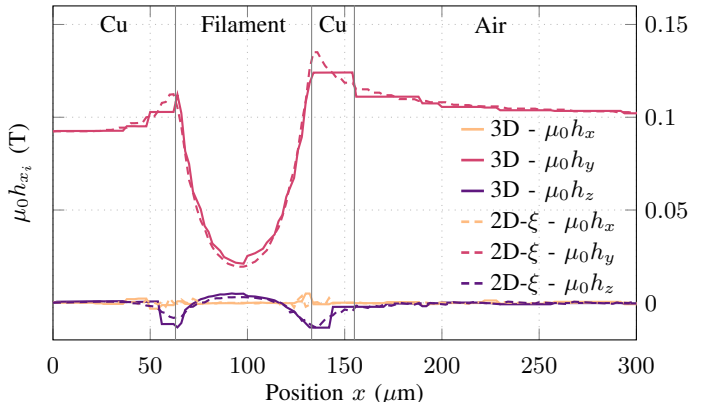


Fig. 14: Magnetic field components along the dashed red line represented in Fig. 13, at $z = 0$, for the 3D and 2D- ξ models with a fine mesh resolution for $\mu_0 h_y = 0.1$ T.

As in the HS-BC case, exploiting the geometrical symmetry allows for a strong reduction of the computational work. It should however be mentioned that the 2D- ξ model with transverse field BC involves double number of degrees of freedom compared to the same model with HS-BC, as two modes are needed to represent the transverse field ($-k$ and k , compared to $k = 0$ only).

The 2D- ξ model still leads to a considerable reduction of DOFs compared to the 3D model. Indeed, taking values of the fine mesh resolution from Table. I, the 3D model involves 145k DOFs whereas the 2D- ξ model with two modes only involves 12k DOFs.

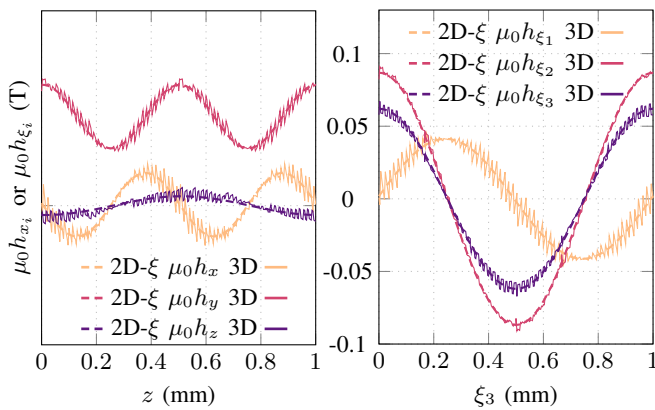


Fig. 15: Magnetic field along the helicoidal fiber of pitch length p , passing at point $\mathbf{x} = (r, 0, 0)$, with $r = R_\ell + 0.8R_f$ (represented by the red dot in Fig. 13), from $z = 0$ to $z = p$, for the 3D and 2D- ξ models for $\mu_0 h_y = 0.1$ T. (Left) Cartesian components of the vectors. (Right) Helicoidal components of the vectors.

B. Application on a 54-filament wire with linear materials

We now consider the 54-filament geometry defined in Fig. 9 but with a linear material in the filaments. We fix the resistivity in the filaments to $\rho_{SC} = 1.81 \times 10^{-15} \Omega\text{m}$ and in the matrix to $\rho_{Cu} = 1.81 \times 10^{-10} \Omega\text{m}$.

Choosing such a low resistivity in filaments leads to an approximated model for superconducting wires at low magnetic fields (below filament saturation). We will see that this linear model reproduces the coupling current dynamics observed in the copper matrix of superconducting wires. The validity of the linear model is however limited to this. It does not describe superconducting hysteresis effects in filaments, and hence does not allow for superconducting loss calculation. Instead, in the following, the computed losses in the filament region will be those of a normal resistive material.

We compute the AC loss induced by a time-varying transverse magnetic field $\mu_0 \mathbf{h} = b_{\max} \sin(\omega t) \hat{e}_y$, with $b_{\max} = 0.1$ T, as a function of the frequency $f = \omega/2\pi$. As in the previous section, BC are such that only the modes $f_{-1}(\xi_3)$ and $f_{+1}(\xi_3)$ are excited (see Eqn. (39) to (42)).

Moreover, because the materials are linear and the excitation is harmonic, the problem can be solved in the frequency domain. To this end, we write the problem in terms of the auxiliary complex quantity $\hat{h}(\xi)$, the phasor of the magnetic field. The phasor is related to the physical magnetic field by $\mathbf{h}(\xi, t) = \Re(\hat{h}(\xi)e^{i\omega t})$, with $i = \sqrt{-1}$, and we replace all time derivatives in the formulation by a multiplication by $i\omega$.

The time-average instantaneous loss density, in W/m^3 , reads, in terms of Cartesian and helicoidal components of the phasor $\hat{\mathbf{j}}$ for the current density:

$$\frac{1}{2} \hat{\mathbf{j}}_{\mathbf{x}}^* (\rho \hat{\mathbf{j}}_{\mathbf{x}}) = \frac{1}{2} \hat{\mathbf{j}}_{\xi}^* \tilde{\rho} \hat{\mathbf{j}}_{\xi}, \quad (44)$$

where $\hat{\mathbf{j}}^*$ denotes the transposed complex conjugate of $\hat{\mathbf{j}}$. Note that both sides of Eq. (44) are real since ρ is a scalar and $\tilde{\rho}$ is a hermitian tensor. The *total loss* per unit length is obtained by integrating Eq. (44) over the whole wire cross section.

We decompose this total loss into separate contributions, which allows for an easier interpretation of the results. The

filament loss is the integral of Eq. (44) on the filament region only. The *coupling loss* is the integral of Eq. (44) on the matrix region only, taking only the in-plane components of $\hat{\mathbf{j}}_{\mathbf{x}}$ into account (the x and y Cartesian components). Finally, the *eddy current loss* is the same but with only the out-of-plane component \hat{j}_z .

We present the results for frequencies ranging from 10^{-2} Hz to 10^5 Hz in Fig. 16 for a pitch length $p = 10$ mm. Values from a 3D reference model are also given for comparison, the agreement with the 2D- ξ model is very good. The current distribution at two distinct frequencies is shown in Fig. 17.

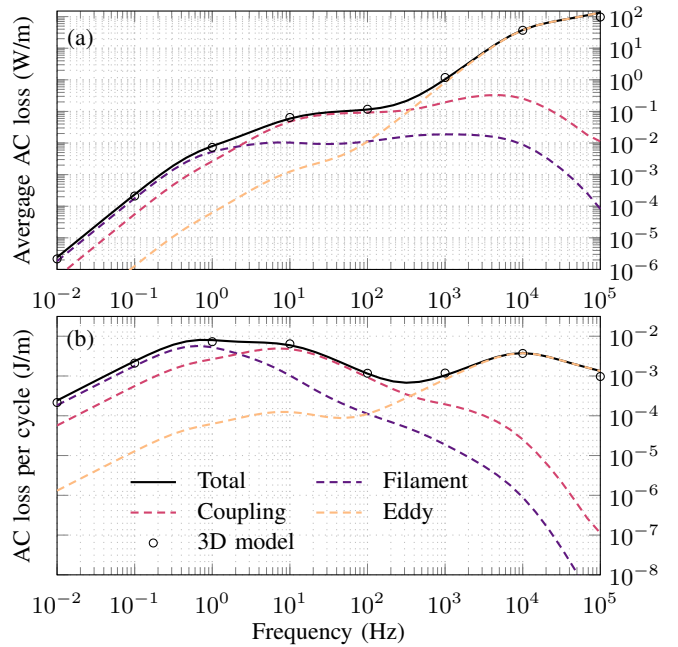


Fig. 16: AC loss as a function of the frequency of an external transverse magnetic field for linear materials and $p = 10$ mm. The total loss as well as separate contributions (filament, coupling, eddy) are shown. The legend is valid for both subfigures. The markers denote the total loss obtained by a 3D model, for verification.

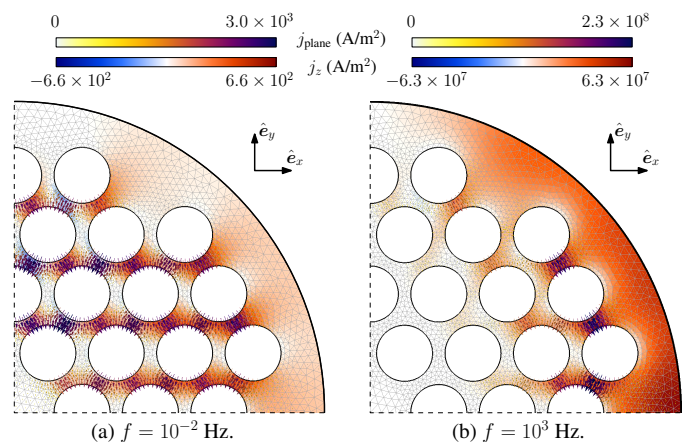


Fig. 17: Real part of the current density distribution in the matrix in transverse magnetic field in harmonic regime. Arrows represent the in-plane x - y -components, and elements are colored as a function of the out-of-plane z -component.

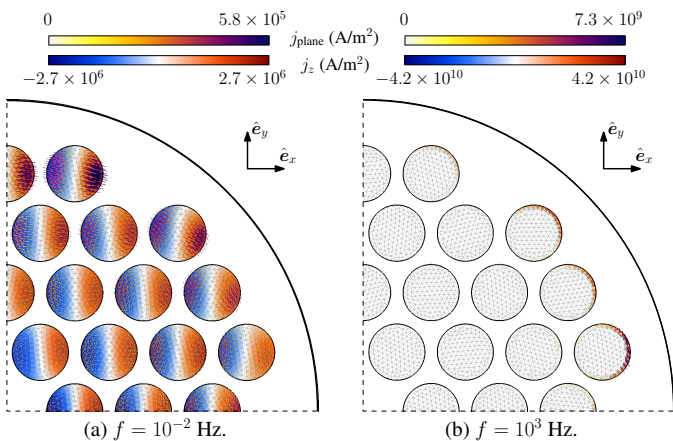


Fig. 18: Real part of the current distribution in the filaments in transverse magnetic in harmonic regime. Arrows represent the in-plane x - y -components, and elements are colored as a function of the out-of-plane z -component.

Figure 16 shows that the dominant loss contribution depends on the frequency. This can be interpreted as follows.

Neglecting the effect of the twist, we expect the peak value of the filament loss to arise when the diffusion skin depth $\delta_{SC} = \sqrt{2\rho_{SC}/\omega\mu}$ is comparable with the radius of the wire R_f . We have $\delta_{SC}/R_f = 1$ for the frequency $f = 0.22$ Hz, which is not too far from the peak in Fig. 16(b).

A change of regime for the eddy current loss per cycle should arise when the skin effect starts to play a role in the matrix. This is expected to happen when the diffusion skin depth $\delta_{Cu} = \sqrt{2\rho_{Cu}/\omega\mu}$ is comparable with the thickness of the outer sheath of the matrix $D_{os} \approx 80 \mu\text{m}$. Here, we have $\delta_{Cu}/D_{os} = 1$ for the frequency $f = 7.2$ kHz, which coincides with the peak in Fig. 16(b). Below this frequency, in the 0.1 kHz to 5 kHz range, most of the field is shielded by currents in the filaments, that are coupled via coupling currents, as discussed below.

Coupling losses are due to currents flowing between the filaments, known as the coupling currents [38]. They are represented by the arrows in Fig. 17. It is worth mentioning that they are on average flowing anti-parallel to the applied magnetic field, as predicted by analytical models [38], [36]. Their dynamics is that of an RL-circuit governed by a time constant τ_c and they contribute to a loss per cycle and per unit length q_{cycle} (J/m). Simplified models propose [36]:

$$\tau_c = \frac{\mu_0}{2\rho_{\text{eff}}} \left(\frac{p}{2\pi}\right)^2, \quad q_{\text{cycle}} = \pi R_w^2 \frac{b_{\text{max}}^2}{2\mu_0} \frac{\pi\omega\tau_c}{(\omega^2\tau_c^2 + 1)} \quad (45)$$

with ρ_{eff} the effective resistivity of the matrix, accounting for the presence of the filaments [2]. In the present case in which we assume no insulation between the filaments and the matrix, assuming the filaments have negligible resistivity, we can estimate ρ_{eff} as follows [39]:

$$\rho_{\text{eff}} = \rho_{Cu} \frac{1 - \lambda}{1 + \lambda}, \quad (46)$$

with λ the filling factor of the filaments in the wire. Here, $\lambda = 0.44$ so that $\tau_c = 23$ ms. The associated frequency is $f_c =$

$(2\pi\tau_c)^{-1} = 7$ Hz, which roughly corresponds to the position of the peak value of the coupling loss per cycle in Fig. 16(b). Below the peak frequency, the filaments are mostly decoupled, as the magnetic field does not change fast enough for large coupling currents to appear. Above the peak frequency, they get more and more coupled, as illustrated in Fig. 18.

As an illustration of the effect of p on the coupling losses, we give in Fig. 19 the total and coupling losses for different values of the pitch length. We can verify the agreement with the analytical prediction Eq. (45): the peak position of the coupling losses scales quadratically with p , affecting the total loss significantly. The curve for a pure copper cylindrical conductor of the same radius R_w , with $\rho_{SC} = \rho_{Cu} = 1.81 \times 10^{-10} \Omega\text{m}$, is given for comparison.

Note that for the pure copper case, we have $\delta_{Cu}/R_w = 1$ for $f = 183$ Hz, which roughly corresponds to the position of the peak of AC loss per cycle.

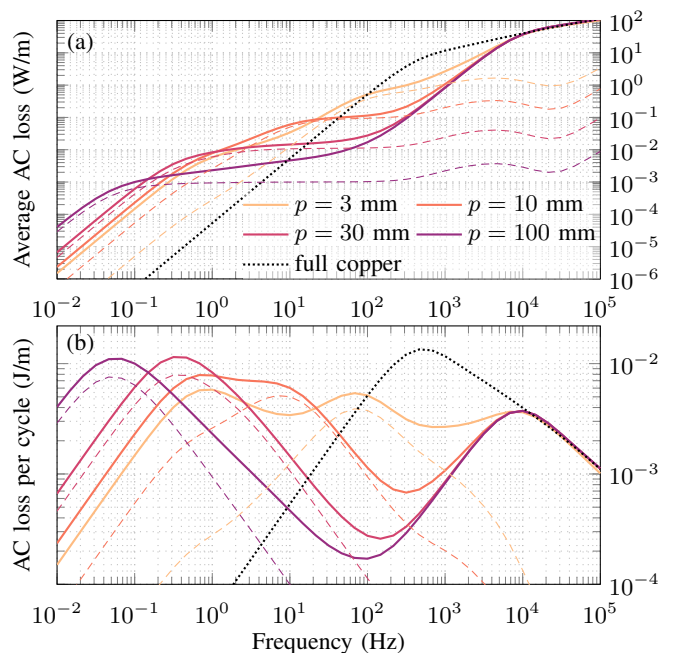


Fig. 19: AC loss as a function of the frequency of an applied transverse magnetic field for linear materials and different pitch lengths. Solid curves represent the total loss. Dashed curves represent the coupling loss only. The main effect of the twist is to shift the coupling loss curves to higher frequencies for decreasing values of p . The total loss for a wire made of copper only (2D model) is given for comparison (dotted curve). The legend is valid for both subfigures.

Figure 19 clearly shows the beneficial effect of twisting the filaments at low frequencies. Wires with smaller pitch length indeed have shorter time constants and are less subject to coupling current losses at low frequencies. It must be mentioned that the twist however does not reduce loss for all frequencies, which is in agreement with experimental measurements, e.g., in [40].

The simple linear model discussed here allows for a qualitative description of coupling current losses that are representative of real superconducting wires for low applied magnetic field only. With superconducting filaments, saturation effects

change the coupling current dynamics for higher field amplitudes [2]. Such effects cannot be reproduced with a linear model.

As already said, the analysis of this linear model must therefore be carried out with caution. Total loss evaluations for superconducting wires cannot be extracted from this model as hysteresis losses of superconducting filaments are not part of the linear model. The inclusion of nonlinear material properties is necessary for such analysis. In the next section, we present the challenges that such an inclusion brings to the helicoidal transformation approach with general BC.

C. Comments for nonlinear materials

In the presence of nonlinear materials, such as superconducting filaments with a power law resistivity described by Eq. (9), mode decoupling is no longer possible with general BC. As derived in the Appendix, the eddy current term of the formulation expands as a double sum on $k, k' \in \mathbb{Z}$ of the terms given by Eq. (51). And each term in Eq. (51) involves the tensor $\tilde{\rho}$. For a superconducting filament, this tensor depends on the full local current density, which couples the modes with different values of $|k|$. A large number of modes in Eq. (30) is therefore likely to be excited by a transverse magnetic field.

As the integral along the ξ_3 -direction can no longer be computed *a priori*, the resulting problem is no longer two-dimensional, which makes it qualitatively different from the 2D- ξ model with linear materials.

To assess the importance of this mode coupling, we can use the 3D model. We show in Fig. 20 the evolution of the magnetic field and the current density along one helicoidal fiber, obtained with the 3D model with the same material parameters as in Section IV, but subject to a transverse magnetic field. As can be seen on the bottom-right plot, the magnetic field in helicoidal coordinates cannot be described only with the two modes $f_{-1}(\xi_3)$ and $f_{+1}(\xi_3)$ as in the linear case. Higher modes are excited.

The amplitude of the different modes can be quantified by a discrete Fourier transform of the magnetic field evolution along this helicoidal fiber. This is illustrated in Fig. 21. Small, but non-negligible contributions are brought by modes $|k| > 1$.

Whether a description with a limited number of modes would lead to satisfying evaluations of losses or not is not an obvious question; knowing *a priori* how many modes should be considered on a new geometry remains an open question. Further investigations in that direction are necessary.

VII. CONCLUSION

In this work, we applied a change of coordinates on the h - ϕ -formulation for modelling multifilamentary wires presenting a helicoidal symmetry. This led to a reduction of the geometrical dimension from 3D to 2D, hence allowing for a substantial gain in terms of computational effort. We separated the study in two steps, depending on the helicoidal symmetry of the boundary conditions (BC). In both cases, we described in details the spatial discretization of finite element fields in helicoidal coordinates. In particular, we emphasized the necessity of using three independent components for the

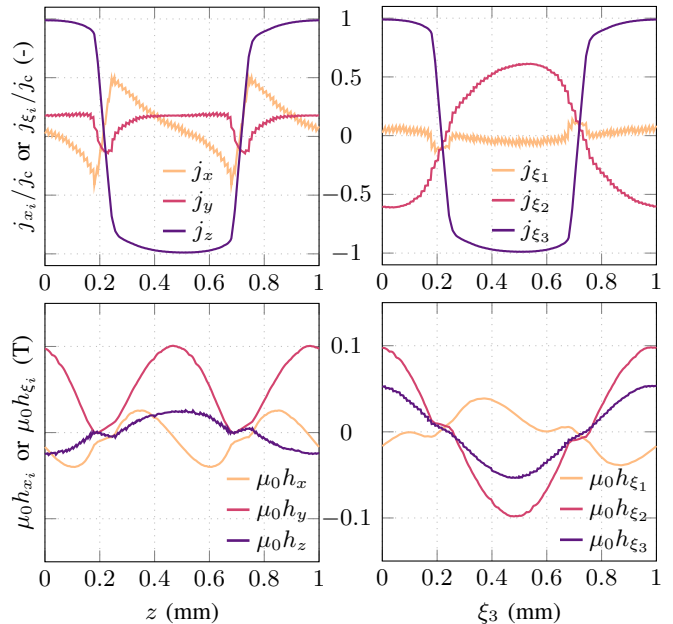


Fig. 20: Current density (up) and magnetic field (down) along the helicoidal fiber of pitch length p , passing through point $\mathbf{x} = (r, 0, 0)$, with $r = R_\ell + 0.8R_f$ from $z = 0$ to p , for a transverse applied magnetic field along \hat{e}_y and Nb-Ti filaments. (Left) Three components of the vectors in the \mathbf{x} -space. (Right) Three components of the vectors in the ξ -space. Solution of the 3D model on a fine mesh with prismatic element in the filaments.

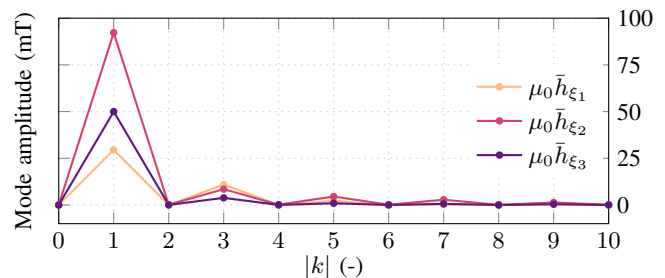


Fig. 21: Amplitudes of the mode contributions for the evolution of the three components of \mathbf{h} in the ξ -space, along the same helicoidal fiber as in Fig. 20. Values are obtained via a fast Fourier transform. Modes for even numbers of k are not excited by a transverse magnetic field.

unknown fields. We then successfully verified our implementation against standard 3D models.

In the case with no external field (e.g. transport current situation only) or with an axial magnetic field, BC are helicoidally symmetric and the method can be directly applied to nonlinear materials. The approach is exact in the sense that no approximation is introduced in the continuous setting. The proposed method can be directly applied on single-layer CORC[®] cables [41] or twisted stacked-tape conductors [42].

In the case of a transverse magnetic field, BC are no longer helicoidally symmetric, but the approach was generalized and applied to linear materials. We presented a study of coupling current induced losses in the harmonic regime, and we finally commented on a possible extension to nonlinear materials. For nonlinear materials with general BC, further investigations are necessary.

APPENDIX

The full h - ϕ -formulation expressed in helicoidal coordinates reads: from an initial solution at $t = 0$, find $\mathbf{h} \in \mathcal{H}(\Omega)$ such that, for $t > 0$ and $\forall \mathbf{h}' \in \mathcal{H}_0(\Omega)$,

$$\begin{aligned} (\partial_t(\tilde{\mu} \mathbf{h}), \mathbf{h}')_{\Omega_{3D}} + (\tilde{\rho} \mathbf{curl} \mathbf{h}, \mathbf{curl} \mathbf{h}')_{\Omega_{c,3D}} \\ = \sum_{i \in C_V} \tilde{V}_i \mathcal{I}_i(\mathbf{h}'), \end{aligned} \quad (47)$$

with $\tilde{\mu}$ and $\tilde{\rho}$ two tensors defined in Eqn. (11) and (12). This formulation is written in the 3D domain Ω_{3D} , not yet reduced to a 2D problem. In the case of non-helicoidally symmetric boundary conditions, the solution \mathbf{h} is not ξ_3 -invariant, and the dimension reduction is not immediate.

Below, we expand the two integral terms of this formulation when the magnetic field $\mathbf{h}(\xi_1, \xi_2, \xi_3)$ is decomposed with Eq. (30) and the modes $f_k(\xi_3)$ defined in Eq. (27). We remind that these modes are orthonormal in the sense of the inner product defined in Eq. (28).

Flux variation term (linear case)

The first term of Eq. (47) expands as the double sum

$$\begin{aligned} \sum_{k=-\infty}^{\infty} \sum_{k'=-\infty}^{\infty} \left(\partial_t(\tilde{\mu} \mathbf{h}_{\parallel,k} f_k), \mathbf{h}'_{\parallel,k'} f_{k'} \right)_{\Omega_{3D}} \\ + \left(\partial_t(\tilde{\mu} \mathbf{h}_{\perp,k} f_k), \mathbf{h}'_{\parallel,k'} f_{k'} \right)_{\Omega_{3D}} \\ + \left(\partial_t(\tilde{\mu} \mathbf{h}_{\parallel,k} f_k), \mathbf{h}'_{\perp,k'} f_{k'} \right)_{\Omega_{3D}} \\ + \left(\partial_t(\tilde{\mu} \mathbf{h}_{\perp,k} f_k), \mathbf{h}'_{\perp,k'} f_{k'} \right)_{\Omega_{3D}}. \end{aligned} \quad (48)$$

Because the decomposition in Eq. (30) separates the variables, we can integrate each individual term along the geometry invariant ξ_3 -direction over one pitch length p . The orthogonality of the modes induces that terms with $k \neq k'$ vanish (provided that μ is not a function of the magnetic field). Dividing the integral by p and using $\|f_k\| = 1$, we get,

$$\begin{aligned} \sum_{k=-\infty}^{\infty} \left(\partial_t(\tilde{\mu} \mathbf{h}_{\parallel,k}), \mathbf{h}'_{\parallel,k} \right)_{\Omega} + \left(\partial_t(\tilde{\mu} \mathbf{h}_{\perp,k}), \mathbf{h}'_{\parallel,k} \right)_{\Omega} \\ + \left(\partial_t(\tilde{\mu} \mathbf{h}_{\parallel,k}), \mathbf{h}'_{\perp,k} \right)_{\Omega} + \left(\partial_t(\tilde{\mu} \mathbf{h}_{\perp,k}), \mathbf{h}'_{\perp,k} \right)_{\Omega}, \end{aligned} \quad (49)$$

where integrals now only have to be performed on a 2D domain. Equations for different values of $|k|$ are uncoupled. In Ω_c^C , the degrees of freedom for $\mathbf{h}_{\perp,k}$ and $\mathbf{h}_{\parallel,-k}$ are linked with each other using Eq. (38).

Eddy current term (linear case)

The second term of Eq. (47) expands as the double sum

$$\begin{aligned} \sum_{k=-\infty}^{\infty} \sum_{k'=-\infty}^{\infty} \left(\tilde{\rho} \mathbf{curl}(\mathbf{h}_{\parallel,k} f_k), \mathbf{curl}(\mathbf{h}'_{\parallel,k'} f_{k'}) \right)_{\Omega_{c,3D}} \\ + \left(\tilde{\rho} \mathbf{curl}(\mathbf{h}_{\perp,k} f_k), \mathbf{curl}(\mathbf{h}'_{\parallel,k'} f_{k'}) \right)_{\Omega_{c,3D}} \\ + \left(\tilde{\rho} \mathbf{curl}(\mathbf{h}_{\parallel,k} f_k), \mathbf{curl}(\mathbf{h}'_{\perp,k'} f_{k'}) \right)_{\Omega_{c,3D}} \\ + \left(\tilde{\rho} \mathbf{curl}(\mathbf{h}_{\perp,k} f_k), \mathbf{curl}(\mathbf{h}'_{\perp,k'} f_{k'}) \right)_{\Omega_{c,3D}}. \end{aligned} \quad (50)$$

Using Eq. (31) for the curl, we get the following lengthy expression for each pair of values $(k, k') \in \mathbb{Z} \times \mathbb{Z}$,

$$\begin{aligned} \left(\tilde{\rho} f_k \mathbf{curl} \mathbf{h}_{\parallel,k}, f_{k'} \mathbf{curl} \mathbf{h}'_{\parallel,k'} \right)_{\Omega_{c,3D}} \\ + \left(\tilde{\rho} \frac{df_k}{d\xi_3} \hat{e}_{\xi_3} \times \mathbf{h}_{\parallel,k}, f_{k'} \mathbf{curl} \mathbf{h}'_{\parallel,k'} \right)_{\Omega_{c,3D}} \\ + \left(\tilde{\rho} f_k \mathbf{curl} \mathbf{h}_{\parallel,k}, \frac{df_{k'}}{d\xi_3} \hat{e}_{\xi_3} \times \mathbf{h}'_{\parallel,k'} \right)_{\Omega_{c,3D}} \\ + \left(\tilde{\rho} \frac{df_k}{d\xi_3} \hat{e}_{\xi_3} \times \mathbf{h}_{\parallel,k}, \frac{df_{k'}}{d\xi_3} \hat{e}_{\xi_3} \times \mathbf{h}'_{\parallel,k'} \right)_{\Omega_{c,3D}} \\ + \left(\tilde{\rho} f_k \mathbf{curl} \mathbf{h}_{\perp,k}, f_{k'} \mathbf{curl} \mathbf{h}'_{\parallel,k'} \right)_{\Omega_{c,3D}} \\ + \left(\tilde{\rho} f_k \mathbf{curl} \mathbf{h}_{\perp,k}, \frac{df_{k'}}{d\xi_3} \hat{e}_{\xi_3} \times \mathbf{h}'_{\parallel,k'} \right)_{\Omega_{c,3D}} \\ + \left(\tilde{\rho} f_k \mathbf{curl} \mathbf{h}_{\parallel,k}, f_{k'} \mathbf{curl} \mathbf{h}'_{\perp,k'} \right)_{\Omega_{c,3D}} \\ + \left(\tilde{\rho} \frac{df_k}{d\xi_3} \hat{e}_{\xi_3} \times \mathbf{h}_{\parallel,k}, f_{k'} \mathbf{curl} \mathbf{h}'_{\perp,k'} \right)_{\Omega_{c,3D}} \\ + \left(\tilde{\rho} f_k \mathbf{curl} \mathbf{h}_{\perp,k}, f_{k'} \mathbf{curl} \mathbf{h}'_{\perp,k'} \right)_{\Omega_{c,3D}}. \end{aligned} \quad (51)$$

In the linear case in which $\tilde{\rho}$ is not a function of the fields, we can integrate each term along the geometry invariant ξ_3 -direction over one pitch length p , divide by p , use the mode property Eq. (29), and exploit the mode orthonormality.

For $k = 0$, because $d_{\xi_3} f_0 = 0$, only terms for $k' = 0$ survive, and they are decoupled from all other terms ($k \neq 0$). These terms are the same as the ones implemented in the case of helicoidally symmetric boundary conditions (HS-BC):

$$\begin{aligned} \left(\tilde{\rho} \mathbf{curl} \mathbf{h}_{\parallel,0}, \mathbf{curl} \mathbf{h}'_{\parallel,0} \right)_{\Omega_c} + \left(\tilde{\rho} \mathbf{curl} \mathbf{h}_{\perp,0}, \mathbf{curl} \mathbf{h}'_{\parallel,0} \right)_{\Omega_c} \\ + \left(\tilde{\rho} \mathbf{curl} \mathbf{h}_{\parallel,0}, \mathbf{curl} \mathbf{h}'_{\perp,0} \right)_{\Omega_c} + \left(\tilde{\rho} \mathbf{curl} \mathbf{h}_{\perp,0}, \mathbf{curl} \mathbf{h}'_{\perp,0} \right)_{\Omega_c}. \end{aligned} \quad (52)$$

For $k \neq 0$, only one term of the sum on k' survives for each term, either $k' = k$, or $k' = -k$. Indeed, Eq. (29) induces the coupling of the modes k and $-k$. For a given value of $k \neq 0$, in Eq. (51), the only terms that remain are

$$\begin{aligned} \left(\tilde{\rho} \mathbf{curl} \mathbf{h}_{\parallel,k}, \mathbf{curl} \mathbf{h}'_{\parallel,k} \right)_{\Omega_c} \\ + \alpha k \left(\tilde{\rho} \hat{e}_{\xi_3} \times \mathbf{h}_{\parallel,k}, \mathbf{curl} \mathbf{h}'_{\parallel,-k} \right)_{\Omega_c} \\ + \alpha(-k) \left(\tilde{\rho} \mathbf{curl} \mathbf{h}_{\parallel,k}, \hat{e}_{\xi_3} \times \mathbf{h}'_{\parallel,-k} \right)_{\Omega_c} \\ + \alpha^2 k^2 \left(\tilde{\rho} \hat{e}_{\xi_3} \times \mathbf{h}_{\parallel,k}, \hat{e}_{\xi_3} \times \mathbf{h}'_{\parallel,k} \right)_{\Omega_c} \\ + \left(\tilde{\rho} \mathbf{curl} \mathbf{h}_{\perp,k}, \mathbf{curl} \mathbf{h}'_{\parallel,k} \right)_{\Omega_c} \\ + \alpha(-k) \left(\tilde{\rho} \mathbf{curl} \mathbf{h}_{\perp,k}, \hat{e}_{\xi_3} \times \mathbf{h}'_{\parallel,-k} \right)_{\Omega_c} \\ + \left(\tilde{\rho} \mathbf{curl} \mathbf{h}_{\parallel,k}, \mathbf{curl} \mathbf{h}'_{\perp,k} \right)_{\Omega_c} \\ + \alpha k \left(\tilde{\rho} \hat{e}_{\xi_3} \times \mathbf{h}_{\parallel,k}, \mathbf{curl} \mathbf{h}'_{\perp,-k} \right)_{\Omega_c} \\ + \left(\tilde{\rho} \mathbf{curl} \mathbf{h}_{\perp,k}, \mathbf{curl} \mathbf{h}'_{\perp,k} \right)_{\Omega_c}. \end{aligned} \quad (53)$$

To these terms, another set needs to be added, with the opposite value of k , $k^* = -k$. In total, this gives eighteen individual terms for the eddy current contribution, for each value of $|k| \neq 0$.

REFERENCES

- [1] W. Carr Jr, "AC loss in a twisted filamentary superconducting wire. I," *Journal of Applied Physics*, vol. 45, no. 2, pp. 929–934, 1974.
- [2] M. N. Wilson, "Superconducting magnets," 1983.
- [3] J. Zhao, Y. Li, and Y. Gao, "3D simulation of AC loss in a twisted multi-filamentary superconducting wire," *Cryogenics*, vol. 84, pp. 60–68, 2017.
- [4] G. Escamez, F. Sirois, V. Lahtinen, A. Stenvall, A. Badel, P. Tixador, B. Ramdane, G. Meunier, R. Perrin-Bit, and C.-E. Bruzek, "3D numerical modeling of AC losses in multifilamentary MgB₂ wires," *IEEE Transactions on Applied Superconductivity*, vol. 26, no. 3, pp. 1–7, 2016.
- [5] G. Escamez, F. Sirois, M. Tousignant, A. Badel, C. Granger, P. Tixador, and C.-É. Bruzek, "Experimental characterization of the constitutive materials of MgB₂ multi-filamentary wires for the development of 3D numerical models," *Superconductor Science and Technology*, vol. 30, no. 3, p. 034008, 2017.
- [6] N. Riva, A. Halbach, M. Lyly, C. Messe, J. Ruuskanen, and V. Lahtinen, "H-phi formulation in Sparselizard combined with domain decomposition methods for modeling superconducting tapes, stacks, and twisted wires," *IEEE Transactions on Applied Superconductivity*, vol. 33, no. 5, pp. 1–5, 2023.
- [7] T. Satiramatekul and F. Bouillault, "Numerical modeling of superconducting filaments for coupled problem," *IEEE transactions on magnetics*, vol. 46, no. 8, pp. 3229–3232, 2010.
- [8] T. Satiramatekul, *Contribution à la modélisation de l'aimantation des brins supraconducteurs*. PhD thesis, Paris 11, 2005.
- [9] A. Kameni, L. Makong, F. Bouillault, and P. J. Masson, "Reduced model to compute AC losses of twisted multifilamentary superconductors," *IEEE Transactions on Applied Superconductivity*, vol. 29, no. 7, pp. 1–6, 2019.
- [10] A. Nicolet, F. Zolla, and S. Guenneau, "Modelling of twisted optical waveguides with edge elements," *The European Physical Journal Applied Physics*, vol. 28, no. 2, pp. 153–157, 2004.
- [11] A. Nicolet and F. Zolla, "Finite element analysis of helicoidal waveguides," in *6th International Conference on Computational Electromagnetics*, pp. 1–3, VDE, 2006.
- [12] A. Nicolet, F. Zolla, Y. O. Agha, and S. Guenneau, "Leaky modes in twisted microstructured optical fibers," *Waves in Random and Complex Media*, vol. 17, no. 4, pp. 559–570, 2007.
- [13] A. Nicolet, A. B. Movchan, S. Guenneau, and F. Zolla, "Asymptotic modelling of weakly twisted electrostatic problems," *Comptes Rendus Mécanique*, vol. 334, no. 2, pp. 91–97, 2006.
- [14] K. Hazim, G. Parent, S. Duchesne, A. Nicolet, and C. Geuzaine, "2D electrostatic modeling of twisted pairs," *COMPEL-The international journal for computation and mathematics in electrical and electronic engineering*, 2021.
- [15] A. Piwonski, J. Dular, R. S. Rezende, and R. Schuhmann, "2D eddy current boundary value problems for power cables with helicoidal symmetry," *IEEE Transactions on Magnetics*, 2023.
- [16] A. Marjamäki, T. Tarhasaari, and P. Rasilo, "Utilizing helicoidal and translational symmetries together in 2-D models of twisted Litz wire strand bundles," *IEEE Transactions on Magnetics*, 2023.
- [17] A. Piwonski, J. Dular, R. S. Rezende, and R. Schuhmann, "Finite element modeling of power cables using coordinate transformations," *IEEE Transactions on Magnetics*, pp. 1–1, 2023.
- [18] A. Stenvall, M. Siahraug, F. Grilli, and F. Sirois, "Computation of self-field hysteresis losses in conductors with helicoidal structure using a 2D finite element method," *Superconductor Science and Technology*, vol. 26, no. 4, p. 045011, 2013.
- [19] V. Lahtinen and A. Stenvall, "Toward two-dimensional simulations of hysteresis losses in partially coupled superconducting wires," *IEEE transactions on applied superconductivity*, vol. 24, no. 3, pp. 1–5, 2013.
- [20] A. Stenvall, T. Tarhasaari, F. Grilli, P. Raunonen, M. Vojenčiak, and M. Pellikka, "Manifolds in electromagnetism and superconductor modelling: Using their properties to model critical current of twisted conductors in self-field with 2D model," *Cryogenics*, vol. 53, pp. 135–141, 2013.
- [21] J. Dular, "Standard and mixed finite element formulations for systems with type-II superconductors," 2023.
- [22] A. Bossavit, *Computational electromagnetism: variational formulations, complementarity, edge elements*. Academic Press, 1998.
- [23] J. Dular, C. Geuzaine, and B. Vanderheyden, "Finite-element formulations for systems with high-temperature superconductors," *IEEE Transactions on Applied Superconductivity*, vol. 30, no. 3, pp. 1–13, 2019.
- [24] P. Dular, C. Geuzaine, F. Henrotte, and W. Legros, "A general environment for the treatment of discrete problems and its application to the finite element method," *IEEE Transactions on Magnetics*, vol. 34, no. 5, pp. 3395–3398, 1998.
- [25] C. Geuzaine and J.-F. Remacle, "Gmsh: A 3D finite element mesh generator with built-in pre-and post-processing facilities," *International journal for numerical methods in engineering*, vol. 79, no. 11, pp. 1309–1331, 2009.
- [26] Y. Ould Agha, *Transformations géométriques réelles et complexes: application à la recherche de modes à pertes dans des fibres optiques microstructurées*. PhD thesis, Aix-Marseille 1, 2007.
- [27] J. D. Jackson, *Classical electrodynamics*. AAPT, 1999.
- [28] J. Rhyner, "Magnetic properties and AC-losses of superconductors with power law current–voltage characteristics," *Physica C: Superconductivity*, vol. 212, no. 3–4, pp. 292–300, 1993.
- [29] A. Bossavit, "Two dual formulations of the 3-D eddy-currents problem," *COMPEL-The international journal for computation and mathematics in electrical and electronic engineering*, 1985.
- [30] R. Brambilla, F. Grilli, and L. Martini, "Development of an edge-element model for AC loss computation of high-temperature superconductors," *Superconductor Science and Technology*, vol. 20, pp. 16–24, nov 2006.
- [31] G. W. Milton, M. Briane, and J. R. Willis, "On cloaking for elasticity and physical equations with a transformation invariant form," *New Journal of Physics*, vol. 8, no. 10, p. 248, 2006.
- [32] A. Nicolet, F. Zolla, Y. Ould Agha, and S. Guenneau, "Geometrical transformations and equivalent materials in computational electromagnetism," *COMPEL-The international journal for computation and mathematics in electrical and electronic engineering*, vol. 27, no. 4, pp. 806–819, 2008.
- [33] A. Bossavit, "Whitney forms: A class of finite elements for three-dimensional computations in electromagnetism," *IEE Proceedings A-Physical Science, Measurement and Instrumentation, Management and Education-Reviews*, vol. 135, no. 8, pp. 493–500, 1988.
- [34] M. Pellikka, S. Suuriniemi, L. Kettunen, and C. Geuzaine, "Homology and cohomology computation in finite element modeling," *SIAM Journal on Scientific Computing*, vol. 35, no. 5, pp. B1195–B1214, 2013.
- [35] B. De Sousa Alves, *3-D Time-Domain Finite Element Modeling of Nonlinear Conductive and Ferromagnetic Thin Films*. PhD thesis, Polytechnique Montréal, 2021.
- [36] A. Campbell, "A general treatment of losses in multifilamentary superconductors," *Cryogenics*, vol. 22, no. 1, pp. 3–16, 1982.
- [37] T. Tominaka, "Calculations using the helical filamentary structure for current distributions of twisted superconducting multifilamentary composites," *Superconductor Science and Technology*, vol. 18, no. 5, p. 634, 2005.
- [38] G. Morgan, "Theoretical behavior of twisted multicore superconducting wire in a time-varying uniform magnetic field," *Journal of Applied Physics*, vol. 41, no. 9, pp. 3673–3679, 1970.
- [39] M. N. Wilson, "NbTi superconductors with low AC loss: A review," *Cryogenics*, vol. 48, no. 7–8, pp. 381–395, 2008.
- [40] K. Kwasnitza, "Scaling law for the ac losses of multifilament superconductors," *Cryogenics*, vol. 17, no. 11, pp. 616–620, 1977.
- [41] Z. Zhu, *Advanced 3D and 2D Modelling of HTS CORC Cable Based on the TA Formulation for the Propulsion System of Hybrid-electric Aircraft*. PhD thesis, University of Bath, 2020.
- [42] M. Takayasu, L. Chiesa, L. Bromberg, and J. Minervini, "Cabling method for high current conductors made of HTS tapes," *IEEE transactions on applied superconductivity*, vol. 21, no. 3, pp. 2340–2344, 2010.